EPJ manuscript No.
(will be inserted by the editor)

arXiv:0712.0354v2 [hep-ph] 7 Aug 2008

$f_0(980)$ meson as a $K\bar{K}$ molecule in a phenomenological Lagrangian approach

Tanja Branz, Thomas Gutsche, and Valery Lyubovitskij[a]

Institut für Theoretische Physik, Universität Tübingen,
Auf der Morgenstelle 14, D-72076 Tübingen, Germany

Received: date / Revised version: date

Abstract. We discuss a possible interpretation of the $f_0(980)$ meson as a hadronic molecule - a bound state of K and $\bar{K}$ mesons. Using a phenomenological Lagrangian approach we calculate the strong $f_0(980) \to \pi\pi$ and electromagnetic $f_0(980) \to \gamma\gamma$ decays. The compositeness condition provides a self-consistent method to determine the coupling constant between f_0 and its constituents, K and $\bar{K}$. Form factors governing the decays of the $f_0(980)$ are calculated by evaluating the kaon loop integrals. The predicted $f_0(980) \to \pi\pi$ and $f_0(980) \to \gamma\gamma$ decay widths are in good agreement with available data and results of other theoretical approaches.

Key words. scalar mesons – hadronic molecule – relativistic meson model – electromagnetic and strong decays

PACS. 13.25.Jx Decays of other mesons 13.40.Hq Electromagnetic decays 14.40.Cs Other mesons with S=C=0, mass < 2.5 GeV 36.10.Gv Mesonic, hyperonic and antiprotonic atoms and molecules

1 Introduction

The understanding of the structure of scalar mesons with masses around 1 GeV is one of the prominent topics in modern hadronic physics. The study of scalar mesons can for example shed light on the problem of the QCD vacuum, *e.g.* to understand the role of gluon configurations and strangeness in the formation of their spectrum. Different interpretations of scalar mesons have been suggested and developed during the last decades [1]. The canonical picture is based on the constituent $q\bar{q}$ structure of scalar mesons. In this vein, by analogy with pseudoscalar and vector mesons, one can organize the low-lying scalar mesons, a triplet of $a_0(980)$, two doublets of $K_0^*(1430)$ and two singlets $f_0(980)$ and $f_0(1370)$, in the form of the $J^P = 0^+$ nonet (see *e.g.* discussion in ref. [2]).

In this paper we focus on the $f_0(980)$ meson. Analyses of the $f_0(980)$ meson as a quarkonium state were performed in several papers (see, *e.g.* refs. [3]-[9]). Different scenarios for the admixture of nonstrange and strange $q\bar{q}$ components have been developed, which range from a pure or dominant $s\bar{s}$ state [3]-[5] to a dominant $n\bar{n} = (u\bar{u} + d\bar{d})/\sqrt{2}$ configuration [6] with a small $s\bar{s}$ mixture of about 10%. Extensions of this scheme by mixing of quarkonia and glueball components have been analyzed in refs. [7, 8]. In [7] it was found that the strong $f_0(980) \to \pi\pi$ decay width is determined by the quarkonium part, while the glueball contribution is small. The dominance of the quarkonium part was also confirmed in ref. [8] in the analysis of the radiative decays of $f_0(980)$. In ref. [10] the existence of scalar multiquark-states was suggested. Scalar mesons (including the $f_0(980)$ meson) have been assigned to the lightest cryptoexotic $q^2\bar{q}^2$ nonet. A further development of the four-quark model for the $f_0(980)$ has been done in [11] and recently in [12]. Properties of the $f_0(980)$ resulting from the $q\bar{q}$ and $q^2\bar{q}^2$ schemes have been critically analyzed. In [13] the structure of the light scalar nonet including $f_0(980)$ was tested using radiative ϕ decays. The authors of Ref. [13] point out the difficulty to distinguish between the $q\bar{q}$ and the $qq\bar{q}\bar{q}$ picture for the light scalar mesons. A possible admixture between $\bar{q}q$ and $qq\bar{q}\bar{q}$ configurations for the low-lying scalar mesons has been considered in ref. [14] using the chiral approach. In refs. [15] the idea of multi-quark states has been put forward to allow for the arrangement of the two quarks and two antiquarks as a bound state of a kaon and a antikaon. Different approaches describing the $f_0(980)$ as a hadronic molecule have already been discussed [15]-[23]. The treatment of the bound state $K\bar{K}$ interaction ranges from simple Gaussian [16] and meson-exchange [18,17] potentials to chiral perturbation theory (ChPT) [19]. Besides this pure configurations, there exist pictures where mixing is included and the $f_0(980)$ incorporates both a $q\bar{q}$ and a $K\bar{K}$ or a glueball component [4,24].

[a] *On leave of absence from the Department of Physics, Tomsk State University, 634050 Tomsk, Russia*

Note, that the question on at least the dominant structure of the $f_0(980)$ meson still remains open. Several comprehensive theoretical studies give completely opposing conclusions. *E.g.*, the unitarised meson model of [5] predicts two complete scalar meson nonets, where the $f_0(980)$ is considered as the $s\bar{s}$ ground state. ref. [4] also describes the $f_0(980)$ as a $q\bar{q}$ state but with a large $K\bar{K}$ component due to the proximity to the $K\bar{K}$ threshold. That is the meson spends most of its time in the virtual $K\bar{K}$ state. The analyses of [25,9] favor the $q\bar{q}$ interpretation of the $f_0(980)$. In particular, ref. [9] predicted two poles close to the $K\bar{K}$ threshold, which suggests that the $f_0(980)$ is a $q\bar{q}$ state with a large $s\bar{s}$ component.

The resonance structure of the $f_0(980)$ was analyzed in [26] by using J/ψ decay data. The f_0 was found to be a conventional Breit-Wigner structure. But the data are also compatible with one pole near threshold, which can be identified with a kaon bound state as mentioned in [17]. However, despite this controversial and detailed discussion concerning the f_0 structure, the $K\bar{K}$ bound state configuration seems to be the dominant contribution [21,22].

In the present paper, the $f_0(980)$ is considered as a pure $K\bar{K}$ molecule in a phenomenological Lagrangian approach. The coupling between the $f_0(980)$ meson and its constituents (K and $\bar{K}$ mesons) is described by the strong interaction Lagrangian. The corresponding coupling constant is determined by the compositeness condition $Z = 0$ [27,3], which implies that the renormalization constant of the hadron wave function is set equal to zero. This condition was first applied in order to study the deuteron as a bound state of proton and neutron [27]. Later this method was successfully applied to low-energy hadron phenomenology. It provides the basic equation for the covariant description of mesons and baryons as composite objects of light and heavy constituent quarks, as well as for glueballs which are bound states of gluons (see *e.g.* discussion in refs. [3,28,29,30,31,32]). Recently the compositeness condition was also used to study the light scalar mesons a_0 and f_0 as $K\bar{K}$ molecules [21,22]. Here, in a first step, we apply our formalism to the study of the strong $f_0(980) \to \pi\pi$ and electromagnetic $f_0(980) \to \gamma\gamma$ decays. In particular, previous determinations of the radiative decay width of the $f_0(980)$, for example when applying the quasi-static approximation, suffer from large uncertainties due to a possible violation of local gauge invariance (for a discussion on this issue see for example [22]). In the present approach such uncertainties are avoided since we use a fully covariant and gauge invariant formalism.

In the future we plan to extend the application to the $a_0(980)$ and investigate a possible $f_0(980) - a_0(980)$ mixture. Recently our Lagrangian approach, based on the compositeness condition, was successfully applied to the study of the $D^*_{s0}(2317)$ and $D_{s1}(2460)$ mesons considered as (DK) and (D^*K) molecules, respectively [33]. In the context of this formalism the strong, electromagnetic and weak decay properties of these states have been evaluated.

In the present paper we proceed as follows. First, in sect. 2, we discuss the basic notions of our approach. We derive the phenomenological mesonic Lagrangian including photons for the treatment of the decay properties of the $f_0(980)$ meson as a $K\bar{K}$ bound state. Then, in sect. 3, we discuss the electromagnetic decay $f_0(980) \to \gamma\gamma$ with the associated diagrams and matrix elements. Special attention will be paid to the proof of electromagnetic gauge invariance. In sect. 4 we turn to the strong decay $f_0 \to \pi\pi$. Numerical results are discussed in sect. 5, followed by a short summary of our results in sect. 6.

2 Approach

In this section we derive and present the formalism for the study of the $f_0(980)$ meson as a hadronic molecule - a bound state of K and $\bar{K}$ mesons. This means that in our approach the $f_0(980)$ does not decay into a $K\bar{K}$ pair. Our framework is based on an interaction Lagrangian describing the coupling between the $f_0(980)$ meson and its constituents as

$$\mathcal{L}_{f_0K\bar{K}}(x) = g_{f_0K\bar{K}}\, f_0(x) \int dy\, \Phi(y^2)\, K^\dagger(x_-)\, K(x_+)\,, \quad (1)$$

where $x_\pm = x \pm y/2$, $K = (K^+, K^0)$ and $K^\dagger = (K^-, \bar{K}^0)$ are the doublets of kaons and antikaons, $g_{f_0K\bar{K}}$ is the $f_0K\bar{K}$ coupling constant. In particular, the assumed molecular structure of the $f_0(980)$ is in terms of particle content of the form

$$|f_0(980)\rangle \;=\; \frac{1}{\sqrt{2}}\,(\,|K^+K^-\rangle + |K^0\bar{K}^0\rangle\,)\,. \quad (2)$$

The correlation function Φ in eq. (1) characterizes the finite size of the $f_0(980)$ meson as a $(K\bar{K})$ bound state and depends on the relative Jacobi coordinate y and the center of mass (CM) coordinate x. The local limit corresponds to the substitution of Φ by the Dirac delta-function: $\Phi(y^2) \to \delta^4(y)$. The Fourier transform of the correlation function reads

$$\Phi(y^2) \;=\; \int \frac{d^4p}{(2\pi)^4}\, e^{-ipy}\, \widetilde{\Phi}(-p^2)\,. \quad (3)$$

Any choice for $\widetilde{\Phi}$ is appropriate as long as it falls off sufficiently fast in the ultraviolet region of Euclidean space to render the Feynman diagrams ultraviolet finite. We employ the Gaussian form

$$\widetilde{\Phi}(p_E^2) \doteq \exp(-p_E^2/\Lambda^2) \quad (4)$$

for the vertex function, where p_E is the Euclidean Jacobi momentum. Here Λ is a size constant, which parametrizes the distribution of kaons inside the f_0 molecule.

The $f_0K\bar{K}$ coupling constant $g_{f_0K\bar{K}}$ is determined by the compositeness condition [27,3], which implies that the renormalization constant of the hadron wave function is set equal to zero:

$$Z_{f_0} = 1 - \Sigma'_{f_0}(M^2_{f_0}) = 0\,. \quad (5)$$

Here $\Sigma'_{f_0}(M^2_{f_0}) = g^2_{f_0K\bar{K}}\Pi'_{f_0}(M^2_{f_0})$ is the derivative of the $f_0(980)$ meson mass operator described by the diagram in

fig. 1 (details of the calculation are given in Appendix A). As we already stressed in the Introduction, this condition has been widely applied.

In order to calculate the strong $f_0(980) \to \pi\pi$ and electromagnetic $f_0(980) \to \gamma\gamma$ decays we need to specify the phenomenological Lagrangian which generates the contributing meson-loop diagrams. The lowest-order Lagrangian $\mathcal{L}$, formulated in terms of the scalar meson $f_0(980)$, pseudoscalar (π, K, $\cdots$), vector (K^*, $\cdots$) mesons and photon fields, is given by:

$$\mathcal{L}(x) = \mathcal{L}_{f_0}(x) + \mathcal{L}^{\rm GI}_{f_0K\bar{K}}(x) + \mathcal{L}_U(x) + \mathcal{L}_W(x)\,, \quad (6)$$

where

$$\mathcal{L}_{f_0}(x) = -\frac{1}{2} f_0(x)(\Box + M^2_{f_0}) f_0(x) \quad (7)$$

is the free Lagrangian of the f_0 meson with $\Box = \partial_\mu\partial^\mu$. $\mathcal{L}^{GI}_{f_0K\bar{K}}$ is the gauge-invariant form of the $f_0K\bar{K}$ interaction Lagrangian, which *i.e.* includes photons via the path integral $I(x,y,P) = \int\limits_y^x dz_\mu A^\mu(z)$ with

$$\mathcal{L}^{\rm GI}_{f_0K\bar{K}}(x) = g_{f_0K\bar{K}} f_0(x) \int dy\, \Phi(y) \times \Big[e^{-ieI(x_+,x_-)}\, K^+(x_+)\, K^-(x_-) + K^0(x_+)\, \bar{K}^0(x_-) \Big]. \quad (8)$$

The term $\mathcal{L}_U$, written as

$$\mathcal{L}_U(x) = \frac{F^2}{4} \langle\, D_\mu U(x) D^\mu U^\dagger(x) + \chi U^\dagger(x) + \chi^\dagger U(x) \,\rangle \quad (9)$$

is the Lagrangian of second-order chiral perturbation theory (ChPT) [34,35] in the three-flavor meson sector [36] and the Lagrangian

$$\mathcal{L}_W(x) = \langle\, -\frac{1}{2}\nabla^\sigma W_{\sigma\mu}\nabla_\nu W^{\nu\mu} + \frac{1}{4} M_V^2 W_{\mu\nu} W^{\mu\nu} + \frac{iG_V}{\sqrt{2}} W_{\mu\nu} u^\mu u^\nu \,\rangle \quad (10)$$

involves vector mesons in the tensorial representation [35, 38,39]. The symbols $\langle\ \rangle$ and $[\ ]$ occurring in above formulas denote the trace over flavor matrices and the commutator, respectively.

Here we use the standard notations of ChPT. The fields of pseudoscalar mesons are collected in the chiral matrix $U = u^2 = \exp(i\sum_i \phi_i\lambda_i/F)$ with $F = F_\pi = 92.4$ MeV being the leptonic decay constant; D_μ is the covariant derivative acting on the chiral field:

$$D_\mu U = \partial_\mu U + i[U,Q]A_\mu + \ldots \quad (11)$$

with Q being the charge matrix of quarks and A_μ is the electromagnetic field; $u_\mu = iu^\dagger D_\mu U u^\dagger$ is the chiral vielbein and $\chi = 2B\mathcal{M} + \cdots$; B is the quark vacuum condensate parameter $B = -\langle 0|\bar{u}u|0\rangle/F^2 = -\langle 0|\bar{d}d|0\rangle/F^2$; $\mathcal{M} = {\rm diag}\{\hat{m}, \hat{m}, m_s\}$ is the mass matrix of current quarks with $\hat{m} = (m_u + m_d)/2$. We work in the isospin limit and rely on the standard picture of chiral symmetry breaking ($B \gg F$). In the leading order of the chiral expansion the masses of pions and kaons are given by $M_\pi^2 = 2\hat{m}B$, $M_K^2 = (\hat{m}+m_s)B$. $W_{\mu\nu} = -W_{\nu\mu} = (\sum_i W_i\lambda_i)_{\mu\nu}/\sqrt{2}$ is the octet of vector fields written in the tensor representation in the terms of antisymmetric tensor fields [35,38,39]; ∇^μ is the covariant derivative acting on vector fields (in our case we restrict ∇^μ to the simple derivative ∂^μ); G_V is the coupling related to the decay constant of a vector meson into two pseudoscalars. With the use of low-energy theorems it can be expressed through the leptonic decay constant F as [40]: $G_V = F/\sqrt{2}$. Finally we comment on the Lagrangian $\mathcal{L}^{\rm GI}_{f_0K\bar{K}}$. As is discussed in detail in refs. [30,31] the presence of vertex form factors in the interaction Lagrangian [like the strong interaction Lagrangian describing the coupling of $f_0(980)$ to its constituents, see eq. (1)] requires special care in establishing gauge invariance. One of the possibilities is provided by a modification of the charged fields, which are multiplied by an exponential containing the electromagnetic field. This procedure was suggested in [41] and applied in ref. [42] and in refs. [30,31, 33]. In our case the fields of charged kaons are modified as

$$K^\pm(y) \to e^{\mp iI(y,x,P)}\, K^\pm(y)\,. \quad (12)$$

By using the substitution (12) we obtain the strong Lagrangian $\mathcal{L}^{\rm GI}_{f_0K\bar{K}}$, which in addition obeys electromagnetic gauge invariance. Note, that for the derivative of the path integral $I(y,x,P) = \int\limits_x^y dz_\mu A^\mu(z)$ we use the path-independent prescription suggested in ref. [41]

$$\lim_{dx^\mu\to 0} dx^\mu \frac{\partial}{\partial x^\mu} I(x,y,P) = \lim_{dx^\mu\to 0} [I(x+dx,y,P') - I(x,y,P)]\,, \quad (13)$$

where the path P' is obtained from P by shifting the endpoint x by dx. Definition (13) leads to the key rule

$$\frac{\partial}{\partial x^\mu} I(x,y,P) = A_\mu(x)\,, \quad (14)$$

which in turn states that the derivative of the path integral $I(x,y,P)$ does not depend on the path P originally used in the definition. The non-minimal prescription (12) is therefore completely equivalent to the minimal substitution (see *e.g.* discussion in ref. [42]). Expanding the gauge exponential in eq. (8) up to second order in the electromagnetic field A_μ we generate nonlocal vertices with a single [fig. 2(a)] and two [fig. 2(b)] photons attached. The derivation of the Feynman rules for such vertices is discussed in detail in Appendix B.

Now we turn to the discussion of the diagrams contributing to the strong $f_0(980) \to \pi\pi$ and electromagnetic $f_0(980) \to \gamma\gamma$ decays. The diagrams which describe the two pion decay $f_0(980) \to \pi\pi$ are shown in fig. 3. The two-point diagram of fig. 3(a) is generated by the $K\bar{K}\pi\pi$ contact interaction, whereas the three-point diagram of fig. 3(b) includes an exchange of the vector meson K^* in

order to take into account rescattering effects. The diagrams describing the electromagnetic $f_0(980) \to \gamma\gamma$ decay are shown in fig. 4. In addition to the diagrams of fig. 4(a) and 4(b), which are generated by the coupling of charged kaons to photons, the restoration of electromagnetic gauge invariance requires the inclusion of the diagrams displayed in figs. 4(c)-4(e). These additional graphs are generated by the vertices shown in figs. 2(a) and 2(b).

Meson loop diagrams are evaluated by using the free meson propagators of K and K^*. The K-meson propagator is given by

$$\begin{aligned} i\,S_K(x-y) &= \langle 0|T\,K(x)\,K^\dagger(y)|0\rangle \\ &= \int \frac{d^4k}{(2\pi)^4 i}\, e^{-ik(x-y)}\ \tilde{S}_K(k)\,, \end{aligned} \tag{15}$$

where

$$\tilde{S}_K(k) = \frac{1}{M_K^2 - k^2 - i\epsilon}\,. \tag{16}$$

For the K^* meson we use the tensorial representation of the chiral Lagrangian (10) with the propagator

$$\begin{aligned} S^W_{K^*;\mu\nu,\alpha\beta}(x-y) &= \langle 0|T\,K^*_{\mu\nu}(x) K^{*\,\dagger}_{\alpha\beta}(y)|0\rangle \\ &= -\frac{1}{M^2_{K^*}} \int \frac{d^4k}{(2\pi)^4 i} \frac{e^{ik\cdot(x-y)}}{M^2_{K^*} - k^2 - i\epsilon} \\ &\times \left[g_{\mu\alpha} g_{\nu\beta}(M^2_{K^*} - k^2) + g_{\mu\alpha} k_\nu k_\beta \right. \\ &\left. - g_{\mu\beta} k_\nu k_\alpha - (\mu \leftrightarrow \nu)\right]. \end{aligned} \tag{17}$$

In the numerical calculations we restrict to the isospin limit and identify the meson masses of the iso-multiplets with the masses of the charged partners [1]

$$\begin{aligned} M_\pi &\equiv M_{\pi^\pm} = 139.57018 \text{ MeV}\,, \\ M_K &\equiv M_{K^\pm} = 493.677 \text{ MeV}\,, \\ M_{K^*} &\equiv M_{K^{*\pm}} = 891.66 \text{ MeV}\,. \end{aligned} \tag{18}$$

Following refs. [21,22] we write the $f_0(980)$-mass in the form

$$M_{f_0} = 2M_K - \epsilon\,, \tag{19}$$

where ϵ represents the binding energy. Further on we will discuss the dependence of observables on ϵ, considered as a free parameter.

3 The electromagnetic decay

In this section we consider the electromagnetic decay $f_0 \to \gamma\gamma$, which proceeds via the charged kaon loop and where all appropriate diagrams are pictured in fig. 4. We derive the transition amplitude in a manifest gauge-invariant way and finally deduce the form factors. In the first part, we consider the local case, which corresponds to a vertex function with $\lim_{\Lambda\to\infty} \widetilde{\Phi}(-k^2) = 1$ in the phenomenological Lagrangian (8). After that we proceed with the nonlocal case keeping the full form of $\widetilde{\Phi}(-k^2)$ in (8), *i.e.* include finite-size effects. As mentioned before, in the local approximation the two-photon decay amplitude is generated by the two diagrams of figs. 4(a) and 4(b). In the nonlocal case we have to include the three additional diagrams of figs. 4(c)-4(e) to restore the full electromagnetic gauge invariance. For the evaluation of the diagrams we follow the procedure developed in refs. [30,31,33,32]. *E.g.* in ref. [31] we present a detailed analysis of the two-photon decay of the light σ-meson, which is similar to the present case. The contribution of each single diagram is not gauge invariant by itself, but the total sum is invariant. Therefore, the calculation of the matrix elements can be simplified by separating each diagram into a gauge invariant part $I^{\mu\nu}_\perp$ and a remainder, denoted by $\delta I^{\mu\nu}$, as

$$I^{\mu\nu} = I^{\mu\nu}_\perp + \delta I^{\mu\nu}\,. \tag{20}$$

This separation can be achieved in the following manner. For the γ-matrices (which only appear in fermionic loops) and vectors with open Lorentz index μ, coinciding with the index of the photon polarization vector $\epsilon^{(\lambda)}_\mu$, one can use the representation (see *e.g.* the discussion in refs. [30, 31,33]):

$$\gamma_\mu = \gamma^\perp_\mu + q_\mu \frac{\not{q}}{q^2}\,, \qquad p_\mu = p^\perp_\mu + q_\mu \frac{pq}{q^2}\,. \tag{21}$$

The sum of all remainder terms cancels (see Appendices C and D). Therefore, the resulting matrix element is only given by the first part in the r.h.s. of (20), from which we can extract the form factors.

The $f_0(980) \to \gamma\gamma$ transition matrix element $\mathcal{M}^{\mu\nu}_{f_0}$ can be written in terms of the Lorentz tensors $b^{\mu\nu}$ and $c^{\mu\nu}$ as

$$\begin{aligned} \mathcal{M}^{\mu\nu}_{f_0} = e^2 \Big\{ & F_{f_0\gamma\gamma}(p^2, q_1^2, q_2^2)\, b^{\mu\nu} \\ & + G_{f_0\gamma\gamma}(p^2, q_1^2, q_2^2)\, c^{\mu\nu} \Big\}. \end{aligned} \tag{22}$$

The tensor structures are given by

$$b^{\mu\nu} = g^{\mu\nu}(q_1 q_2) - q_1^\nu q_2^\mu\,, \tag{23}$$

$$c^{\mu\nu} = g^{\mu\nu} q_1^2 q_2^2 + q_1^\mu q_2^\nu (q_1 q_2) - q_1^\mu q_1^\nu q_2^2 - q_2^\mu q_2^\nu q_1^2\,, \tag{24}$$

where q_1 and q_2 refer to the four-momenta of the photons. Note, that the part of the matrix element containing the form factor $G_{f_0\gamma\gamma}(p^2,\, q_1^2,\, q_2^2)$ vanishes, when at least one of the photons is on-shell, since $c^{\mu\nu} = 0$.
The two photon decay width

$$\Gamma(f_0 \to \gamma\gamma) = \frac{\pi}{4} \alpha^2 M^3_{f_0} g^2_{f_0\gamma\gamma} \tag{25}$$

is expressed in terms of the coupling constant

$$g_{f_0\gamma\gamma} = F_{f_0\gamma\gamma}(M^2_{f_0},\, 0,\, 0)\,, \tag{26}$$

which in turn is related to the form factor $F_{f_0\gamma\gamma}$.

3.0.1 Local case

In the local approximation we only have to consider the diagrams of figs. 4(a) and 4(b). Using the decomposition (20) one can show that the resulting matrix element is given by the gauge-invariant part of the diagram of fig. 4(a) only with

$$I^{L\,\mu\nu}_{\Delta,\perp}(q_1,\,q_2) = \int \frac{d^4k}{\pi^2 i}\,(2k+q_1)^{\mu}_{\perp q_1}\,(2k-q_2)^{\nu}_{\perp q_2} \times S_K\,(k+q_1)\;S_K\,(k-q_2)\;S_K(k)\,, \quad (27)$$

which is ultraviolet (UV) finite. An important point is that noninvariant parts of figs. 3(a) and 3(b) cancel each other (see details in Appendix C). The evaluation of eq. (27) yields (the explicit calculation is carried out in Appendix C):

$$F^L_{\Delta}(p^2,q_1^2,q_2^2) = \int\limits_0^1 d^3\alpha\,\delta(1-\sum_{i=0}^{3}\alpha_i)\frac{4\alpha_1\alpha_2}{D}\,, \quad (28)$$

where $D = M_K^2 - p^2\alpha_1\alpha_2 - q_1^2\alpha_1\alpha_3 - q_2^2\alpha_2\alpha_3$. Later on, we also analyze the electromagnetic $f_0(980)$ form factors for different values of the photon virtuality in the Euclidean region by expressing q_1^2 and q_2^2 as $q_1^2 = -Q^2(1+\omega)/2$ and $q_2^2 = -Q^2(1-\omega)/2$. A similar analysis of the electromagnetic π and σ-meson form factors was performed previously in refs. [43] and [29,31,32].

The expression for the coupling constant $g_{f_0\gamma\gamma}$, resulting from [29], is given by

$$g_{f_0\gamma\gamma} = \frac{g_{f_0K\bar{K}}}{8\pi^2}\int\limits_0^1 d\alpha_1\int\limits_0^1 d\alpha_2\,\frac{4\alpha_1\alpha_2(1-\alpha_1)^2}{M_K^2 - M_{f_0}^2\alpha_1\alpha_2(1-\alpha_1)} = \frac{g_{f_0K\bar{K}}}{8\pi^2}R_{f_0\gamma\gamma}\,, \quad (29)$$

where

$$R_{f_0\gamma\gamma} = \left(\frac{\arcsin\xi}{\xi}\right)^2 - 1\,,\; \xi = \frac{M_{f_0}}{2M_K} = 1 - \frac{\epsilon}{2M_K}\,. \quad (30)$$

In the local limit (see Appendix A) the coupling constant $g_{f_0K\bar{K}}$ is expressed in the form

$$\frac{1}{g^2_{f_0K\bar{K}}} = \frac{R_{f_0}}{8\pi^2 M^2_{f_0}} \quad (31)$$

with

$$R_{f_0} = \frac{\arcsin\xi}{\xi\sqrt{1-\xi^2}} - 1\,. \quad (32)$$

Finally, the expression for the $f_0 \to \gamma\gamma$ decay width reads as follows

$$\Gamma(f_0\to\gamma\gamma) = \frac{\alpha^2}{8\pi}\,\frac{R^2_{f_0\gamma\gamma}}{R_{f_0}}M_{f_0}\,, \quad (33)$$

which agrees with the result of [21,22].

3.0.2 Nonlocal case

Now we turn to the nonlocal interaction case and discuss the evaluation of the corresponding Feynman diagrams. In this case we have to incorporate all diagrams shown in fig. 4. In Appendix B we outline the derivation of the Feynman rules for the nonlocal vertices with a single [fig. 2(a)] and two [fig. 2(b)] photon lines attached; these nonlocal vertices have to be included to guarantee full gauge invariance both on the level of the Lagrangian and the matrix elements. For further details we refer to our earlier paper [31]. In analogy to the local case, the form factors $F(p^2,q_1^2,q_2^2)$ and $G(p^2,q_1^2,q_2^2)$ can be extracted from the gauge invariant parts of the respective diagrams

$$I^{\mu\nu}(q_1,q_2) \equiv I^{\mu\nu}_{\perp}(q_1,q_2) = F(p^2,q_1^2,q_2^2)\,b^{\mu\nu} + G(p^2,q_1^2,q_2^2)\,c^{\mu\nu}\,. \quad (34)$$

The individual contributions are given by:

$$\begin{aligned} & I^{\mu\nu}_{\triangle_\perp}(q_1,q_2) \\ &= \int \frac{d^4k}{\pi^2 i}\,\widetilde{\Phi}(-k^2)\,(2k+q_2)^{\mu}_{\perp q_1}\,(2k-q_1)^{\nu}_{\perp q_2} \\ &\times S_K\left(k+\frac{p}{2}\right)\,S_K\left(k-\frac{p}{2}\right)\,S_K\left(k+\frac{q}{2}\right) \\ &= F_{\triangle}(p^2,q_1^2,q_2^2)b^{\mu\nu} + G_{\triangle}(p^2,q_1^2,q_2^2)c^{\mu\nu} \quad (35) \\ & I^{\mu\nu}_{\mathrm{bub}_\perp}(q_1,q_2) \\ &= -\int \frac{d^4k}{\pi^2 i}\int\limits_0^1 dt\,\widetilde{\Phi}'(-x(0,q_1))\,2k^{\mu}_{\perp q_1}k^{\nu}_{\perp\,q_2} \\ &\times S_K\left(k+\frac{q_2}{2}\right)\,S_K\left(k-\frac{q_2}{2}\right) \\ &+(q_1\leftrightarrow q_2,\,\mu\leftrightarrow\nu) \\ &= F_{\mathrm{bub}}(p^2,q_1^2,q_2^2)b^{\mu\nu} + G_{\mathrm{bub}}(p^2,q_1^2,q_2^2)c^{\mu\nu} \quad (36) \end{aligned}$$

and

$$\begin{aligned} & I^{\mu\nu}_{\mathrm{tad}_\perp}(q_1,q_2) \\ &= \int\frac{d^4k}{\pi^2 i}\,S_K(k)\int\limits_0^1 dt\left(-\frac{c^{\mu\nu}}{4\,q_1^2\,q_2^2}\left(\widetilde{\Phi}'(-x(0,p))\right.\right. \\ &\left.+\widetilde{\Phi}'(-x(0,q))\right) + t\int\limits_0^1 dl\left(k+\frac{q_2}{2}\right)^{\mu}_{\perp\,q_1}k^{\nu}_{\perp q_2} \\ &\left.\times\left(\widetilde{\Phi}''(-x(q_1,q_2)) + \widetilde{\Phi}''(-x(-q_1,q_2))\right)\right) \\ &+(q_1\leftrightarrow q_2,\,\mu\leftrightarrow\nu) \\ &= F_{\mathrm{tad}_\perp}(p^2,\,q_1^2,\,q_2^2)b^{\mu\nu} + G_{\mathrm{tad}_\perp}(p^2,\,q_1^2,\,q_2^2)c^{\mu\nu}\,, \quad (37) \end{aligned}$$

where

$$\begin{aligned} x(q_1,q_2) &= k^2 + kt(l\,q_1+q_2) + \frac{t}{4}(l\,q_1^2 + 2\,l\,q_1q_2 + q_2^2)\,, \\ q &= q_2 - q_1\,. \quad (38) \end{aligned}$$

Here, eqs. (35), (36) and (37) correspond to the triangle diagrams of figs. 4(a) and 4(b), to the bubble diagrams of figs. 4(c) and 4(d), and to the tadpole diagram of fig. 4(e). The evaluation of these structure integrals is performed in Appendix D without referring to a specific functional form of the vertex function $\widetilde{\Phi}(-k^2)$. Then the decay width for $f_0(980) \to \gamma\gamma$ is calculated in analogy to the local case. We discuss the numerical results in sect. 5.

4 The strong decay

In this section we discuss the features of the $f_0(980) \to \pi\pi$ decay. The two-pion decay width is determined by the expression

$$\begin{aligned}\Gamma_{f_0\pi\pi} &= \Gamma_{f_0\pi^+\pi^-} + \Gamma_{f_0\pi^0\pi^0} = \frac{3}{2}\Gamma_{f_0\pi^+\pi^-} \\ &= \frac{3}{32\pi}\frac{g^2_{f_0\pi\pi}}{M_{f_0}}\sqrt{1-\frac{4M_\pi^2}{M_{f_0}^2}}\,, \end{aligned} \tag{39}$$

where the coupling constant $g_{f_0\pi\pi}$ is given by

$$g_{f_0\pi\pi} = g_{f_0\pi^+\pi^-} = 2g_{f_0\pi^0\pi^0} = G(M_{f_0}^2, M_\pi^2, M_\pi^2) \tag{40}$$

defined by the effective Lagrangian $\mathcal{L}_{f_0\pi\pi} = \frac{1}{2}g_{f_0\pi\pi}f_0\boldsymbol{\pi}^2$. Here, $G(p^2, q_1^2, q_2^2)$ is the structure integral of the $f_0 \to \pi\pi$ transition, which is conventionally split into the two terms $G^{(a)}(p^2, q_1^2, q_2^2)$ and $G^{(b)}(p^2, q_1^2, q_2^2)$. They refer to the contributions of the diagrams of figs. 3(a) and 3(b), respectively, with

$$G(p^2, q_1^2, q_2^2) = G^{(a)}(p^2, q_1^2, q_2^2) + G^{(b)}(p^2, q_1^2, q_2^2)\,, \tag{41}$$

$$\begin{aligned}G^{(a)}(p^2, q_1^2, q_2^2) &= \frac{g_{f_0K\bar{K}}}{3\,F^2}\int\frac{d^4k}{(2\pi)^4 i}\,\widetilde{\Phi}(-k^2) \\ &\times \frac{M_K^2 + \frac{5}{4}p^2 - k^2}{(M_K^2 - k_+^2)(M_K^2 - k_-^2)}\,, \end{aligned} \tag{42}$$

$$\begin{aligned}G^{(b)}(p^2, q_1^2, q_2^2) &= \frac{g_{f_0K\bar{K}}}{2\,F^2}\int\frac{d^4k}{(2\pi)^4 i}\,\widetilde{\Phi}(-k^2) \\ &\times\Big\{\frac{(k_+^2 - q_1^2)(k_+ - q_1)(k_- - q_2)}{(M_K^2 - k_+^2)(M_K^2 - k_-^2)(M_{K^*}^2 - (k_+ - q_1)^2)} \\ &- \frac{(k_+ - q_1)^2(k_+ + q_1)(k_- - q_2)}{(M_K^2 - k_+^2)(M_K^2 - k_-^2)(M_{K^*}^2 - (k_+ - q_1)^2)}\Big\}\,, \end{aligned} \tag{43}$$

where $k_\pm = k \pm p/2$. Here we substitute $G_V = F/\sqrt{2}$ in the expression for $G^{(b)}(p^2, q_1^2, q_2^2)$.

It is worth to note, that the sum of the diagrams of fig. 3 contributing to the coupling $g_{f_0\pi\pi}$ can be approximated by a single diagram - the triangle diagram of fig. 3(b) with the exchanged K^* meson propagator in vectorial representation. In particular, we remind that the free Lagrangian of the K^* meson in the vector representation is written in the form:

$$\mathcal{L}_V = -\frac{1}{2}K^{*\dagger}_{\mu\nu}K^{*\,\mu\nu} + M^2_{K^*}K^{*\dagger}_\mu K^{*\mu}, \tag{44}$$

where $K^*_{\mu\nu} = \partial_\mu K^*_\nu - \partial_\nu K^*_\mu$. Then for the sake of comparison between the two different representation it is convenient to write down the propagator in the vector representation as a T-product of $K^*_{\mu\nu}$:

$$\begin{aligned}S^V_{K^*;\mu\nu,\alpha\beta}(x-y) &= \langle 0|T\,K^*_{\mu\nu}(x)K^{*\,\dagger}_{\alpha\beta}(y)|0\rangle \\ &= -\frac{1}{M^2_{K^*}}\int\frac{d^4k}{(2\pi)^4 i}\frac{e^{ik\cdot(x-y)}}{M^2_{K^*} - k^2 - i\epsilon} \\ &\times\left[g_{\mu\alpha}k_\nu k_\beta - g_{\mu\beta}k_\nu k_\alpha - (\mu\leftrightarrow\nu)\right]. \end{aligned} \tag{45}$$

As was stressed in ref. [39], the propagators $S^V_{K^*;\mu\nu,\alpha\beta}$ and $S^W_{K^*;\mu\nu,\alpha\beta}$ differ by the contact term contained in the tensorial propagator:

$$\begin{aligned}S^W_{K^*;\mu\nu,\alpha\beta}(x) &= S^V_{K^*;\mu\nu,\alpha\beta}(x) \\ &+ \frac{i}{M^2_{K^*}}[g_{\mu\alpha}g_{\nu\beta} - g_{\mu\beta}g_{\nu\alpha}]\,\delta^4(x)\,. \end{aligned} \tag{46}$$

Using identity (46) one can show that the contribution of the diagram fig. 3(b) in tensorial representation is given by the sum of the graph of fig. 3(b) in vectorial representation plus a graph, which is diagrammatically described by fig. 3(a), but has opposite sign and a different numerator in comparison to the structure integral $G^{(a)}(p^2, q_1^2, q_2^2)$. Latter graph results from the contact term contained in the propagator (46), leading to the collapse of the K^* line in fig. 3(b) to a point. In other words, the sum of diagrams of fig. 3 in tensorial representation generates a leading term which corresponds to the diagram of fig. 3(b) in vectorial representation. In addition we obtain a term resulting effectively from the difference of two graphs of the type fig. 3(a), but with different numerators in the expression. Numerically it is found that in the last term these two contributions almost compensate each other. Therefore, we effectively obtain a contribution of the graph of fig. 3(b) only, but now with the K^* meson propagator written in vectorial representation.

As an alternative we also present a technique how to include non-perturbative pion-pion interaction near the $K\bar{K}$ threshold by following the method of a chiral unitarity approach. By defining an effective coupling $\widetilde{g}_{K\bar{K}\pi\pi}$ between the intermediate kaons and the $\pi\pi$ pair we can write down the phenomenological Lagrangian

$$\mathcal{L}_{K\bar{K}\pi\pi} = \widetilde{g}_{K\bar{K}\pi\pi}\bar{K}K\boldsymbol{\pi}\cdot\boldsymbol{\pi}\,.$$

Within this approach the $f_0\pi\pi$ coupling and consequently the width is defined in terms of this effective coupling constant

$$\begin{aligned}g_{f_0\pi\pi} &= \frac{g_{f_0K\bar{K}}\widetilde{g}_{K\bar{K}\pi\pi}}{(4\pi)^2} \\ &\times\int\frac{d^4k}{\pi^2 i}\,\widetilde{\Phi}(-k^2)\frac{1}{M_K^2 - \left(k + \frac{p}{2}\right)^2}\frac{1}{M_K^2 - \left(k - \frac{p}{2}\right)^2}\,. \end{aligned}$$

A full analysis of this ansatz goes beyond the scope of the present paper. However, by using the two-pion decay width $\Gamma(f_0 \to \pi\pi)$=19.5 MeV derived in [37] within the framework of a chiral unitarity approach, we can estimate the effective coupling $\widetilde{g}_{K\bar{K}\boldsymbol{\pi\pi}}$ around 10 GeV.

5 Numerical analysis

5.1 Coupling constant $g_{f_0K\bar{K}}$

First we present our results for the $g_{f_0K\bar{K}}$ coupling constant, both in the local and nonlocal case. In figs. 5 and 6 we demonstrate the sensitivity of the $g_{f_0K\bar{K}}$ coupling on variations of the free parameters. In fig. 5 we give $g_{f_0K\bar{K}}$ as a function of the binding energy ϵ for the local case. In fig. 6 $g_{f_0K\bar{K}}$ is drawn as a function of two parameters, ϵ and the size parameter Λ of the vertex function. For typical values of $\epsilon = 2M_K - 980$ MeV $\simeq 7.4$ MeV (corresponding to $M_{f_0} = 980$ MeV) and $\Lambda = 1$ GeV the results for the coupling constant are

$$g_{f_0K\bar{K}} = 2.90 \text{ GeV} \quad \text{(local case)} \tag{47}$$

and

$$g_{f_0K\bar{K}} = 3.09 \text{ GeV} \quad \text{(nonlocal case)}\,. \tag{48}$$

5.2 The electromagnetic decay

In figs. 7 and 8 we present our results for the coupling constant $g_{f_0\gamma\gamma}$ for the local and the nonlocal case. In particular, in fig. 7 we consider the local limit and draw $g_{f_0\gamma\gamma}$ as a function of the binding energy ϵ. The results for $g_{f_0\gamma\gamma}$ in the nonlocal case in dependence on the two parameters ϵ and Λ is presented in fig. 8. For the typical values of $\epsilon = 7.4$ MeV and $\Lambda = 1$ GeV we obtain both for the coupling constant $g_{f_0\gamma\gamma}$ and the decay width $\Gamma(f_0 \to \gamma\gamma)$ the results

$$\begin{aligned} g_{f_0\gamma\gamma} &= 0.086 \text{ GeV}^{-1}\,, \\ \Gamma(f_0 \to \gamma\gamma) &= 0.29 \text{ keV} \quad \text{(local case)} \end{aligned} \tag{49}$$

and

$$\begin{aligned} g_{f_0\gamma\gamma} &= 0.079 \text{ GeV}^{-1}\,, \\ \Gamma(f_0 \to \gamma\gamma) &= 0.25 \text{ keV} \quad \text{(nonlocal case)}\,. \end{aligned} \tag{50}$$

These results are in very good agreement with the new average $\Gamma(f_0 \to \gamma\gamma) = 0.29^{+0.07}_{-0.09}$ keV quoted by PDG 2007 [1] and recent data presented by the Belle Collaboration [44]: $\Gamma(f_0 \to \gamma\gamma) = 0.205^{+0.095+0.147}_{-0.083-0.117}$ keV. Our results also agree with previous results by the Crystal Ball Collaboration [45] ($\Gamma_{\gamma\gamma} = 0.31 \pm 0.14 \pm 0.09$ keV) and by MARK II at SLAC [46] ($\Gamma_{\gamma\gamma} = 0.29 \pm 0.07 \pm 0.12$ keV).

In table 1 we compare our predictions (49) for the two-photon decay width of the f_0 meson with other theoretical approaches [48,50,51,22,3,11,49]. Quark-antiquark models predict similar results for $\Gamma(f_0 \to \gamma\gamma)$. For example, predictions in the quarkonium interpretation range from $\Gamma(f_0 \to \gamma\gamma)$=0.24 keV [3] to values of 0.33 keV [49] with an intermediate result of $0.28^{+0.09}_{-0.13}$ keV [50]. The result of the four-quark model [11] with $\Gamma(f_0 \to \gamma\gamma)$=0.27 keV lies in the range set by our local and nonlocal predictions.

Previous determinations in the context of hadronic molecule interpretations of $\Gamma(f_0 \to \gamma\gamma) = 0.20$ keV [51] and 0.22 ± 0.07 [22] lie at the lower side of our results. The difference in results can to some extent be explained by using different values for the meson masses (*e.g.* as in ref. [22]).

At this level, present data on $\Gamma(f_0 \to \gamma\gamma)$ cannot serve to uniquely deduce the dominant configuration of the $f_0(980)$. Furthermore, a recent amplitude analysis [47] involving high statistics data by BELLE [44] allows for values for $\Gamma(f_0 \to \gamma\gamma)$ from 0.10 to 0.54 keV. Therefore, a more precise determination of the width, narrowing down the region of the possible values, would affect the determination of the dominant configuration.

For the $f_0 \to \gamma\gamma$ decay properties finite size effects only play a role at the level of about 10% (for the decay width) when both photons are on-shell (in this point we completely agree with the conclusions of ref. [22]). The finite size effects become essential for a nontrivial virtuality of one of the photons. The same qualitative conclusion about the importance of finite size effects was known before from the analysis of the electromagnetic transition form factors of the π- and the light σ-meson (see refs. [43] and [29,31]). In particular, it was shown (see *e.g.* discussion in refs. [29,31]) that a local coupling between the π- or the light σ-meson and their constituent quarks leads to the wrong asymptotics, that is $\ln^2(Q^2/m^2)/(2Q^2)$, of the transition form factor, when one of the photons is on-shell while the other one has an Euclidean off-shell momentum squared. Such an asymptotics is in contradiction to the QCD-prediction for the $\pi^0\gamma\gamma^*$ form factor of $1/Q^2$ [52]. A similar situation holds for the electromagnetic f_0 form factor. In fig. 9 we indicate the form factor $F_{f_0\gamma\gamma^*}(Q^2) = F_{f_0\gamma\gamma}(M_{f_0}^2, -Q^2, 0)$ for the transition $f_0 \to \gamma\gamma^*$ with a real and a virtual photon of Euclidean momentum squared $-Q^2$. To demonstrate the sensitivity of this form factor on finite-size effects we plot the result both for the local case and for the nonlocal vertex function with different values for $\Lambda = 0.7, 1$ and 1.3 GeV. The additional bubble and tadpole diagrams of figs. 4(c)-(e), which result from the nonlocal interaction, only give a minor contribution to the dominant one of the triangle diagram. The curve corresponding to the local case lies considerably higher than those for the nonlocal case (including its asymptotic behavior at large values of Q^2), even for moderate values of Q^2. Moreover, the electromagnetic form factor shows a sensitivity of about 20% in the Q^2 range considered with respect to variations of Λ or to the finite size of f_0. Clearly, an experimental determination of $F_{f_0\gamma\gamma^*}(Q^2)$ would help in possibly identifying the underlying structure of the $f_0(980)$. $F_{f_0\gamma\gamma^*}(Q^2)$ can be approximated by a monopole function. Actually, this was also to be expected from the analysis of analogous form factors for the π^0 and the light σ meson (see [43] and [29, 31]) with:

$$F_{f_0\gamma\gamma^*}(Q^2) = \frac{F_{f_0\gamma\gamma^*}(0)}{1 + Q^2/\Lambda^2_{f_0\gamma\gamma^*}}\,, \tag{51}$$

where $F_{f_0\gamma\gamma^*}(0) \equiv g_{f_0\gamma\gamma}$. The scale parameter $\Lambda_{f_0\gamma\gamma^*}$ can be related to the slope of the $F_{f_0\gamma\gamma^*}(Q^2)$ form factor de-

fined as

$$\langle r^2 \rangle \;=\; -6\,\frac{F'_{f_0\gamma\gamma^*}(0)}{F_{f_0\gamma\gamma^*}(0)}\,, \tag{52}$$

where

$$F'_{f_0\gamma\gamma^*}(0) = \left.\frac{\partial F_{f_0\gamma\gamma^*}(Q^2)}{\partial Q^2}\right|_{Q^2=0}. \tag{53}$$

From eqs. (51) and (52) we deduce the relation between $\langle r^2\rangle$ and $\Lambda_{f_0\gamma\gamma^*}$ with

$$\langle r^2\rangle = \frac{6}{\Lambda^2_{f_0\gamma\gamma^*}}\,. \tag{54}$$

Therefore, the slope $\langle r^2\rangle$ has a quite clear physical meaning - it is related to the charge distribution of the constituents K^+ and K^- inside the f_0 molecule. Our prediction for $\langle r^2\rangle$ at values of $\epsilon = 7.4$ MeV and $\Lambda = 1$ GeV is

$$\langle r^2\rangle = 0.15 \text{ fm}^2\,. \tag{55}$$

It constraints the scale parameter to a value of $\Lambda_{f_0\gamma\gamma^*} = 1.26$ GeV. Good agreement in the full Q^2 range with the exact result of the nonlocal case with parameters $\epsilon = 7.4$ MeV and $\Lambda = 1$ GeV is obtained with a monopole function of scale parameter $\Lambda_{f_0\gamma\gamma^*} \simeq 1.4$ GeV (for comparison it is also plotted in fig. 9), which is a bit larger than the value of 1.26 GeV deduced near Q^2=0.

To improve the $F_{f_0\gamma\gamma^*}$ form factor we can also include finite size effects in the $K\bar{K}\gamma$ couplings, *i.e.* by replacing the local $K\bar{K}\gamma$ vertices by the electromagnetic kaon form factors

$$F_{K\bar{K}\gamma}(Q^2) = \frac{1}{1+Q^2/\Lambda^2_{K\bar{K}\gamma}}\,.$$

The size parameter $\Lambda_{K\bar{K}\gamma}$ is related to the slope of the kaon electromagnetic form factor (52) which can be deduced from the charged kaon radius $\langle r^2_{K^\pm}\rangle = \frac{6}{\Lambda_{K\bar{K}\gamma}}$ which we take from [1]. The charge radius $r_{K^\pm} = 0.56$ fm leads to a value of $\Lambda_{K\bar{K}\gamma} = 0.863$ GeV. The additional form factors suppress the estimates for the coupling $g_{f_0\gamma\gamma^*}$ when the off-shell behavior of the photons is studied (see fig. 10). However, the finite size effects are still apparent. The decay properties for real photons are not affected by the monopole form factor since $F_{K\bar{K}\gamma}(Q^2)\big|_{Q^2=0} = 1$.

5.3 The strong decay

The experimental results for the dominant decay process $f_0(980) \to \pi\pi$ are spread out in a large region. Consequently, PDG 2007 [1] indicates a wide range for the total width from 40-100 MeV. Recently, the Belle Collaboration [44] reported the result of $\Gamma(f_0 \to \pi\pi) = 51.3^{+20.8\,+13.2}_{-17.7\,-3.8}$ MeV.

The coupling constant $g_{f_0\pi\pi}$ and, accordingly, the decay width (39) depend sensitively on the cut-off parameter Λ, since without the correlation function $\widetilde{\Phi}(-k^2)$ the diagrams of fig. 3 are UV divergent. In fig. 11 we present our results for the coupling $g_{f_0\pi\pi}$ as a function of ϵ and Λ. Again the results for the coupling constant $g_{f_0\pi\pi}$ and the decay width $\Gamma(f_0 \to \pi\pi)$ are given for the usual values of $\epsilon = 7.4$ MeV and $\Lambda = 1$ GeV as

$$g_{f_0\pi\pi} = 1.53 \text{ GeV} \tag{56}$$

and

$$\Gamma(f_0 \to \pi\pi) = 69 \text{ MeV}\,, \tag{57}$$

consistent with current observation.

In table 2 we compare our results to data and results of other theoretical approaches. Predictions of $q\bar{q}$ models for $\Gamma(f_0 \to \pi\pi)$ span a large range of values from 20 MeV [3] to 56 − 58 MeV [24], which sensitively depend on the nonstrange flavor content. For the dynamically generated $f_0(980)$ of ref. [37] a somewhat low value of $\Gamma(f_0 \to \pi\pi)$=18.2 MeV is obtained.

It is interesting to note that the analysis of the KLOE collaboration on $\phi \to f_0(980)\gamma \to \pi^+\pi^-\gamma$ [53] results in the ratio of couplings with $R = g^2_{f_0K^+K^-}/g^2_{f_0\pi\pi} = 2.2 - 2.8$ in agreement with our prediction of

$$R = \frac{g^2_{f_0K^+K^-}}{g^2_{f_0\pi\pi}} = 2.28\,. \tag{58}$$

6 Summary

We have discussed the electromagnetic $f_0 \to \gamma\gamma$ and the strong $f_0 \to \pi\pi$ decays of the $f_0(980)$ considered as a hadronic $K\bar{K}$ molecule in a phenomenological Lagrangian approach. Our approach is manifestly Lorentz and gauge invariant and is based on the use of the compositeness condition. We have only one model parameter Λ, which is related to the size of the $K\bar{K}$ distribution in the f_0 meson and, therefore, controls finite-size effects. In addition, we studied the sensitivity on the detailed value of the binding energy ϵ.

We showed that finite-size effects only moderately influence the $f_0 \to \gamma\gamma$ decay properties (coupling constant and decay width), when both photons are on-shell (in this point we completely agree with the conclusions of ref. [22]), while these effects become essential for a nontrivial virtuality of one of the photons. Also, the consideration of the finite size of the f_0 meson in the molecular $K\bar{K}$ picture is sufficient to explain the strong $f_0 \to \pi\pi$ decay properties. More precise experimental information on the $f_0 \to \pi\pi$ decay, and more so for the $F_{f_0\gamma\gamma^*}(Q^2)$ form factor can certainly help in at least constraining the molecular $K\bar{K}$ content of the $f_0(980)$. Given the current model approach and the status of experimental data, the strong and electromagnetic decay properties of the $f_0(980)$ can be fully explained in a molecular $K\bar{K}$ interpretation of this state. The success in explaining the decay modes of the $f_0(980)$ does at this level not exclude possible alternative explanations, such as $q\bar{q}$ or compact $q^2\bar{q}^2$ configurations.

To elaborate further on a possible molecular structure of the $f_0(980)$ in future we plan to include in our analysis the $a_0(980)$ meson and its mixing with the $f_0(980)$. Using the approach developed here we intend to analyze different strong, radiative and weak production and decay processes involving the $f_0(980)$ and $a_0(980)$ mesons. A full treatment of these observables can possibly shed more light on the structure of these peculiar scalar states.

Acknowledgments

We thank C. Hanhart and S. Scherer for useful discussions. This work was supported by the DFG under contracts FA67/31-1 and GRK683. This research is also part of the EU Integrated Infrastructure Initiative Hadronphysics project under contract number RII3-CT-2004-506078 and President grant of Russia "Scientific Schools" No. 871.2008.2.

A Mass operator of $f_0(980)$ and coupling constant $g_{f_0K\bar{K}}$

The $f_0(980)$ mass operator $\Pi_{f_0}(p^2)$ reads as

$$\Pi_{f_0}(p^2) = 2\int \frac{d^4k}{(2\pi)^4 i}\,\widetilde{\Phi}^2(-k^2)\,S_K(k_+)\,S_K(k_-)\,, \quad (59)$$

where $k_\pm = k + p/2$. To simplify the illustration of the calculation technique we restrict ourselves to the isospin limit. After introducing the Feynman α-parametrization with

$$\frac{1}{AB} = \int\limits_0^1 d\alpha \frac{1}{(A\alpha + B(1-\alpha))^2} \quad (60)$$

and by applying the Cauchy theorem for the vertex function squared [29]

$$\widetilde{\Phi}^2(-k^2) = \oint \frac{dz}{2\pi i}\frac{\widetilde{\Phi}^2(-z)}{z-k^2} \quad (61)$$

we get

$$\Pi_{f_0}(p^2) = \frac{1}{8\pi^2}\int\limits_0^1 d\alpha \int \frac{d^4k}{\pi^2 i}\oint \frac{dz}{2\pi i}\frac{\widetilde{\Phi}(-z)}{z-k^2} \times \frac{1}{(M_K^2 - (k+r)^2 + r^2 - p^2/4)^2}\,, \quad (62)$$

where $r = p(1-2\alpha)/2$. Then, using the integral representation

$$\frac{1}{AB^2} = 2\int\limits_0^\infty d\beta\,\frac{\beta}{(A+B\beta)^3} \quad (63)$$

and performing the integration over the loop momentum k we obtain

$$\Pi(p^2) = \frac{1}{8\pi^2}\int\limits_0^1 d\alpha \int\limits_0^\infty \frac{d\beta\beta}{(1+\beta)^2}\,\widetilde{\Phi}^2(\Delta)\,, \quad (64)$$

where

$$\Delta = \beta\left(M_K^2 - p^2\frac{1+4\alpha\beta(1-\alpha)}{4(1+\beta)}\right). \quad (65)$$

Finally, by evaluating the derivative of the mass operator with respect to p^2 for the on-mass-shell value of $p^2 = M_{f_0}^2$ we calculate the coupling constant $g_{f_0K\bar{K}}$ by use of the compositeness condition (5) with:

$$\frac{1}{g_{f_0K\bar{K}}^2} = \frac{1}{32\pi^2\Lambda^2}\int\limits_0^1 d\alpha \int\limits_0^\infty \frac{d\beta\beta^2}{(1+\beta)^3}\,(1+4\alpha\beta(1-\alpha)) \times (1+4\alpha\beta(1-\alpha))\left(-\frac{d\widetilde{\Phi}^2(\Delta)}{d\Delta}\right)\Big|_{p^2=M_{f_0}^2}. \quad (66)$$

In the local limit, that is $\Lambda \to \infty$, eq. (66) becomes

$$\frac{1}{g_{f_0K\bar{K}}^2} = \frac{R_{f_0}}{8\pi^2 M_{f_0}^2} \quad (67)$$

with

$$R_{f_0} = \frac{\arcsin\xi}{\xi\sqrt{1-\xi^2}} - 1\,. \quad (68)$$

B Feynman rules for the nonlocal vertices

Restoration of electromagnetic gauge invariance in the strong $f_0K\bar{K}$ interaction Lagrangian modifies the coupling to charged kaons as

$$\mathcal{L}(x) = g_{f_0K\bar{K}} f_0(x)\int dy\,\Phi(y)\,e^{-ieI(x_+,x_-)} \times K^+(x_+)\,K^-(x_-)\,, \quad (69)$$

where $x_\pm = x \pm y/2$.
After expansion of the gauge exponentials up to second order in the electromagnetic field we generate the nonlocal vertices containing a single photon [fig. 2(a)] and two photon lines [fig. 2(b)]. In our procedure we follow ref. [31] where we obtain for the single-photon vertex

$$e\left(k+\frac{q_1}{4}\right)^\mu \int\limits_0^1 dt\,\widetilde{\Phi}'(x(0,q_1)) + (q_1 \leftrightarrow q_2,\ \mu\leftrightarrow\nu)\,, \quad (70)$$

and for the two-photon vertex

$$\begin{aligned} &- e^2\frac{g^{\mu\nu}}{4}\int\limits_0^1 dt\left(\widetilde{\Phi}'(-x(0,p)) + \widetilde{\Phi}'(-x(0,q))\right) \\ &+ \int\limits_0^1 dt\,t\int\limits_0^1 dl\left(\widetilde{\Phi}''(-x(q_1,q_2))\left(k+q_{21}^+\right)^\mu\left(k+\frac{q_4}{4}\right)^\nu\right. \\ &\left.+\,\widetilde{\Phi}''(-x(-q_1,q_2))\left(k+q_{21}^-\right)^\mu\left(k+\frac{q_2}{4}\right)^\nu\right) \\ &+ (q_1\leftrightarrow q_2,\ \mu\leftrightarrow\nu)\,, \end{aligned} \quad (71)$$

where

$$\begin{aligned} x(q_1,q_2) &= k^2 + kt(l\,q_1+q_2) + \frac{t}{4}(l\,q_1^2 + 2\,l\,q_1q_2 + q_2^2) \\ q_{ij}^{\pm} &= \frac{q_i}{2} \pm \frac{q_j}{4} \\ q &= q_2 - q_1\,. \end{aligned} \tag{72}$$

C Form factors and gauge invariance of local diagrams

We divide the hadron loop integral

$$\begin{aligned} I_{\triangle}^{L\,\mu\nu}(q_1,q_2) = \int \frac{d^4k}{\pi^2 i}\,(2k+q_1)^{\mu}\,(2k-q_2)^{\nu} \\ \times\; S(k+q_1)\,S(k-q_2)\,S(k)\,, \end{aligned} \tag{73}$$

represented by the diagram in fig. 4(a), into a gauge invariant part and the remainder term

$$\begin{aligned} & I_{\triangle_\perp}^{L\,\mu\nu}(q_1,q_2) + \delta I_{\triangle}^{L\,\mu\nu}(q_1,q_2) \\ &= \int \frac{d^4k}{\pi^2 i}(2k+q_1)^{\mu}_{\perp\,q_1}\,(2k-q_2)^{\nu}_{\perp\,q_2} \\ &\times S(k+q_1)S(k-q_2)S(k) \\ &+ \left(\frac{c^{\mu\nu}}{q_1^2q_2^2} - g^{\mu\nu}\right) \int \frac{d^4k}{\pi^2 i} S(k+q_1)\,S(k-q_2)\,. \end{aligned} \tag{74}$$

Here and in the following (Appendices C and D) we only deal with the propagator of charged kaons. We therefore drop in the following the subscript K^+ in the symbol of the propagator.

The second diagram of fig. 4(b) gives

$$I_{\circ}^{L\,\mu\nu}(q_1,q_2) = g^{\mu\nu} \int \frac{d^4k}{\pi^2 i} S(k+q_1)\,S(k-q_2)\,, \tag{75}$$

where (75) and the last term in (74) cancel each other. Therefore, we can easily derive the form factors

$$\begin{aligned} & I_{\triangle_\perp}^{L\,\mu\nu}(q_1,q_2) \\ &= \int \frac{d^4k}{\pi^2 i}\,(2k+q_1)^{\mu}_{\perp\,q_1}\,(2k-q_2)^{\nu}_{\perp\,q_2} \\ &\times S(k+q_1)\,S(k-q_2)\,S(k) \\ &+ \frac{c^{\mu\nu}}{q_1^2q_2^2} \int \frac{d^4k}{\pi^2 i}\,S(k+q_1)S(k-q_2) \\ &= F_{\triangle,\,L}(p^2,q_1^2,q_2^2)\,b^{\mu\nu} + G_{\triangle,\,L}(p^2,q_1^2,q_2^2)\,c^{\mu\nu}\,. \end{aligned} \tag{76}$$

By introducing the Feynman α-parameters and using dimensional regularization we obtain

$$F_{\triangle}^{L}(p^2,q_1^2,q_2^2) = \int_0^1 d^3\alpha\,\delta(1-\sum_{i=1}^3\alpha_i)\,\frac{4\alpha_1\alpha_2}{D}\,, \tag{77}$$

$$\begin{aligned} G_{\triangle}^{L}(p^2,q_1^2,q_2^2) = \frac{1}{q_1^2q_2^2} \int_0^1 d^3\alpha\,\delta(1-\sum_{i=1}^3\alpha_i) \\ \times \left(2\ln\frac{D}{D_0} - \frac{4\alpha_1\alpha_2}{D}q_1q_2\right)\,, \end{aligned} \tag{78}$$

where

$$\begin{aligned} D &= M_K^2 - p^2\alpha_1\alpha_2 - q_1^2\alpha_1\alpha_3 - q_2^2\alpha_2\alpha_3\,, \\ D_0 &= M_K^2 - p^2\alpha_1\alpha_2\,. \end{aligned} \tag{79}$$

D Form factors and gauge-invariance of the nonlocal diagrams

D.1 Triangle diagram

In Appendix C we saw that there are two diagrams which belong to the leading-order term illustrated in fig. 4. In complete analogy to the local case we write down the Feynman integral and split it into a gauge invariant and a remainder term. The first diagram of fig. 4(a) gives

$$\begin{aligned} & I_{\triangle}^{\mu\nu}(q_1,q_2) \\ &= \int \frac{d^4k}{\pi^2 i}\,\widetilde{\Phi}(-k^2)\,(2k+q_2)^{\mu}\,(2k-q_1)^{\nu} \\ &\times S\left(k+\frac{p}{2}\right)\,S\left(k-\frac{p}{2}\right)\,S\left(k+\frac{q}{2}\right) \\ &= \int \frac{d^4k}{\pi^2 i}\,\widetilde{\Phi}(-k^2)\,(2k+q_2)^{\mu}_{\perp\,q_1}\,(2k-q_1)^{\nu}_{\perp\,q_2} \\ &\times S\left(k+\frac{p}{2}\right)\,S\left(k-\frac{p}{2}\right)S\left(k+\frac{q}{2}\right) \\ &+ \int \frac{d^4k}{\pi^2 i}\widetilde{\Phi}\left(-\left(k-\frac{q_2}{2}\right)^2\right)\left(\frac{2k^{\mu}_{\perp q_1}q_2^{\nu}}{q_2^2} + \frac{q_1^{\mu}q_2^{\nu}}{q_1^2q_2^2}kq_1\right) \\ &\times S\left(k+\frac{q_1}{2}\right)S\left(k-\frac{q_1}{2}\right) \\ &- \int \frac{d^4k}{\pi^2 i}\widetilde{\Phi}\,(-k^2)\left(g^{\mu\nu} - \frac{c^{\mu\nu}}{q_1^2q_2^2}\right)S\left(k+\frac{p}{2}\right)S\left(k-\frac{p}{2}\right) \\ &- \int \frac{d^4k}{\pi^2 i}\widetilde{\Phi}\left(-\left(k+\frac{q_1}{2}\right)^2\right)\left(\frac{2q_1^{\mu}k^{\nu}_{\perp q_2}}{q_1^2} + \frac{q_1^{\mu}q_2^{\nu}}{q_1^2q_2^2}kq_2\right) \\ &\times S\left(k+\frac{q_2}{2}\right)S\left(k-\frac{q_2}{2}\right)\,. \end{aligned} \tag{80}$$

The second diagram of fig. 4(b) contributes

$$I_{\circ}^{\mu\nu}(q_1,q_2) = g^{\mu\nu}\int \frac{d^4k}{\pi^2 i}\,\widetilde{\Phi}(-k^2)\,S\left(k-\frac{p}{2}\right)S\left(k+\frac{p}{2}\right)\,.$$

By writing down the invariant part of the integrals in terms of the tensor structures $b^{\mu\nu}$ and $c^{\mu\nu}$, one obtains the form factors

$$\begin{aligned} & F_{\triangle_\perp}(p^2,q_1^2,q_2^2) \\ &= -\int_0^1 d^3\alpha\,\delta\left(1-\sum_{i=1}^3\alpha_i\right)\int_0^1 \frac{dtt^2}{(1-t)^2} \\ &\times\widetilde{\Phi}'(\Delta_1)\,(1-2t\alpha_3+t^2\alpha_{132}\alpha_{231})\,, \end{aligned} \tag{81}$$

$$\begin{aligned} & G_{\triangle_\perp}(p^2,q_1^2,q_2^2) \\ &= \frac{q_1q_2}{q_1^2q_2^2}\int_0^1 d^3\alpha\,\delta\left(1-\sum_{i=1}^3\alpha_i\right)\int_0^1 \frac{dtt^2}{(1-t)^2} \\ &\times\left(-2\widetilde{\Phi}(\Delta_1) + \widetilde{\Phi}'(\Delta_1)\,\frac{1-2t\alpha_3+t^2\alpha_{132}\alpha_{231}}{1-t}\right), \end{aligned} \tag{82}$$

where

$$\Delta_1 = \frac{t}{1-t}\bigg(M_K^2 - \frac{p^2}{4}(\alpha_{123} + t\alpha_{132}\alpha_{231}) - \frac{q_1^2\alpha_3}{2}(1-t\alpha_{231}) - \frac{q_2^2\alpha_3}{2}(1-t\alpha_{132})\bigg) \quad (83)$$

where $\alpha_{ijk} = \alpha_i + \alpha_j - \alpha_k$.

The remainder term reads as

$$\begin{aligned}
&\delta I_{\triangle}^{\mu\nu}(q_1,q_2) \\
&= \int \frac{d^4k}{\pi^2 i}\,\widetilde{\Phi}(-k^2) \\
&\times\bigg(\frac{q_1^\mu q_2^\nu}{q_1^2 q_2^2}\left(S\left(k+\frac{q}{2}\right) - S\left(k-\frac{p}{2}\right)\right) \\
&-\frac{q_1^\mu (2k-q_1)^\nu}{q_1^2}\, S\left(k+\frac{q}{2}\right)\, S\left(k-\frac{p}{2}\right) \\
&+\frac{(2k+q_2)^\mu q_2^\nu}{q_2^2}\, S\left(k+\frac{q}{2}\right)\, S\left(k+\frac{p}{2}\right)\bigg). \qquad (84)
\end{aligned}$$

D.2 Bubble diagram

By writing the Feynman rule for nonlocal vertices, derived in Appendix B, and separating the perpendicular term, we have

$$\begin{aligned}
&I_{\rm bub}^{\mu\nu}(q_1,q_2) \\
&= -2\int \frac{d^4k}{\pi^2 i}\int_0^1 dt\,\widetilde{\Phi}'(-x(0,q_1))\left(k+\frac{q_1}{4}\right)^\mu k^\nu \\
&\times S\left(k+\frac{q_2}{2}\right)\, S\left(k-\frac{q_2}{2}\right) \\
&+(q_1 \leftrightarrow q_2,\ \mu\leftrightarrow\nu) \\
&= -2\int \frac{d^4k}{\pi^2 i}\int_0^1 dt\,\widetilde{\Phi}'(-x(0,q_1))\, k^\mu_{\perp\, q_1} k^\nu_{\perp\, q_2} \\
&\times S\left(k+\frac{q_2}{2}\right)\, S\left(k-\frac{q_2}{2}\right) \\
&+2\int \frac{d^4k}{\pi^2 i}\,\frac{\widetilde{\Phi}(-(k+\frac{q_1}{2})^2) - \widetilde{\Phi}(-k^2)}{kq_1 + \frac{q_1^2}{4}} \\
&\times S\left(k+\frac{q_2}{2}\right) S\left(k-\frac{q_2}{2}\right) \\
&\times\bigg(\left(k+\frac{q_1}{4}\right)^\mu q_2^\nu\,\frac{kq_2}{q_2^2} + q_1^\mu k^\nu\,\frac{\left(k+\frac{q_1}{4}\right)q_1}{q_1^2} \\
&-\ q_1^\mu q_2^\nu \frac{\left(k+\frac{q_1}{4}\right)q_1}{q_1^2 q_2^2} kq_2\bigg) \\
&+(q_1 \leftrightarrow q_2,\ \mu\leftrightarrow\nu) \qquad (85)
\end{aligned}$$

$$\begin{aligned}
&F_{\rm bub_\perp}(p^2,q_1^2,q_2^2) \\
&= \frac{1}{2}\int_0^1 dtt\int_0^1 d\alpha(2\alpha-1)\int_0^\infty \frac{d\beta\beta^2}{(1+\beta)^4}\,\widetilde{\Phi}'(\Delta_2) \\
&+(q_1 \leftrightarrow q_2,\ \mu\leftrightarrow\nu)\,, \qquad (86) \\
&G_{\rm bub_\perp}(p^2,q_1^2,q_2^2) = \frac{1}{q_1^2 q_2^2}\int_0^1 dt\int_0^1 d\alpha\int_0^\infty \frac{d\beta\beta}{(1+\beta)^4} \\
&\times\left\{ \widetilde{\Phi}(\Delta_2) + \frac{1}{2}\,t\,\beta\,(2\alpha-1)\,\widetilde{\Phi}'(\Delta_2)\,q_1 q_2\right\} \\
&+(q_1 \leftrightarrow q_2,\ \mu\leftrightarrow\nu)\,, \qquad (87)
\end{aligned}$$

where

$$\begin{aligned}
\Delta_2 = M_K^2\beta + p^2\,\frac{t\beta(1-2\alpha)}{4(1+\beta)} - q_1^2\,\frac{t(1-t+2\beta(1-\alpha))}{4(1+\beta)} \\
- q_2^2\,\frac{\beta(1+t(1-2\alpha)+4\alpha\beta(1-\alpha)))}{4(1+\beta)}\,. \qquad (88)
\end{aligned}$$

The remainder term is given by

$$\begin{aligned}
&\delta I_{\rm bub}^{\mu\nu}(q_1,q_2) \\
&= \frac{q_1^\mu}{q_1^2}\int\frac{d^4k}{\pi^2 i}\,\widetilde{\Phi}(-k^2)\left(\frac{q_2^\nu}{2q_2^2}\left(S\left(k-\frac{p}{2}\right) - S\left(k+\frac{q}{2}\right)\right)\right. \\
&\left.+2(k-\frac{q_1}{2})^\nu S\left(k+\frac{q}{2}\right) S\left(k-\frac{p}{2}\right)\right) \\
&+\frac{q_1^\mu}{q_1^2}\int\frac{d^4k}{\pi^2 i}\,S(k)\left(\widetilde{\Phi}\left(-\left(k+\frac{q}{2}\right)^2\right)\left(\frac{(k-q_{12}^-)^\nu}{(k-q_{12}^-)q_2}\right.\right. \\
&\left.-\frac{q_2^\nu}{2q_2^2}\right) - \widetilde{\Phi}\left(-\left(k+\frac{p}{2}\right)^2\right)\left(\frac{(k+q_{12}^+)^\nu}{(k+q_{12}^+)q_2} - \frac{q_2^\nu}{2q_2^2}\right) \\
&\left.+\widetilde{\Phi}\left(-\left(k+\frac{q_1}{2}\right)^2\right)\left(\frac{(k+q_{12}^+)^\nu}{(k+q_{12}^+)q_2} - \frac{(k+q_{12}^-)^\nu}{(k+q_{12}^-)q_2}\right)\right) \\
&+\ (q_1 \leftrightarrow q_2,\ \mu\leftrightarrow\nu)\,. \qquad (89)
\end{aligned}$$

D.3 Tadpole diagram

We apply the same procedure as for the bubble diagram and write down the Feynman integral

$$I_{\rm tad}^{\mu\nu}(q_1,q_2) = \int\frac{d^4k}{\pi^2 i}\,S(k)\Lambda^{\mu\nu}\,, \qquad (90)$$

where

$$\begin{aligned}\Lambda^{\mu\nu} &= -\frac{g^{\mu\nu}}{4}\int_0^1 dt\left(\widetilde{\Phi}'(-x(0,\,p))\right.\\ &\left.+\,\widetilde{\Phi}'(-x(0,\,q))\right)\\ &+\int_0^1 dt\,t\int_0^1 dl\left(\widetilde{\Phi}''(-x(q_1,\,q_2))\;\left(k+q_{21}^{+}\right)^{\mu}\right.\\ &\left.+\,\widetilde{\Phi}''(-x(-q_1,\,q_2))\left(k+q_{21}^{-}\right)^{\mu}\right)\left(k+\frac{q_2}{4}\right)^{\nu}\\ &+(q_1\leftrightarrow q_2,\;\mu\leftrightarrow\nu)\\ &= I^{\mu\nu}_{\mathrm{tad}_\perp}+\delta I^{\mu\nu}_{\mathrm{tad}}\,. \end{aligned}\tag{91}$$

By using

$$g^{\mu\nu}=g^{\mu\nu}_{\perp}+\left(\frac{q_1^{\mu}q_1^{\nu}}{q_1^2}+\frac{q_2^{\mu}q_2^{\nu}}{q_2^2}-\frac{q_1^{\mu}q_2^{\nu}\,q_1q_2}{q_1^2q_2^2}\right)\tag{92}$$

we can separate the gauge invariant part

$$\begin{aligned}&I^{\mu\nu}_{\mathrm{tad}_\perp}(q_1,q_2)\\ &=\int\frac{d^4k}{\pi^2 i}\,S(k)\left(\left(k+\frac{q_2}{2}\right)^{\mu}_{\perp q_1}k^{\nu}_{\perp q_2}\right.\\ &\times\int_0^1 dt\,t\int_0^1 dl\,\left(\widetilde{\Phi}''(-x(q_1,\,q_2))+\widetilde{\Phi}''(-x(-q_1,\,q_2))\right)\\ &\left.-\frac{c^{\mu\nu}}{4q_1^2q_2^2}\int_0^1 dt\,\left(\widetilde{\Phi}'(-x(0,\,p))+\widetilde{\Phi}'(-x(0,\,q))\right)\right)\\ &+(q_1\leftrightarrow q_2,\;\mu\leftrightarrow\nu)\,.\end{aligned}\tag{93}$$

from which we derive the form factors

$$\begin{aligned}&F_{\mathrm{tad}_\perp}(p^2,q_1^2,q_2^2)\\ &=\frac{1}{4}\int_0^1 dtt^2\int_0^1 dll\int_0^\infty\frac{d\beta}{(1+\beta)^3}\\ &\times\left(\widetilde{\Phi}'(\Delta_3)-\widetilde{\Phi}'(\Delta_4)\right)\left(\frac{t}{1+\beta}-1\right)\\ &+(q_1\leftrightarrow q_2,\;\mu\leftrightarrow\nu)\,,\end{aligned}\tag{94}$$

$$\begin{aligned}&G_{\mathrm{tad}_\perp}(p^2,q_1^2,q_2^2)\\ &=\frac{1}{4q_1^2q_2^2}\int_0^1 dtt\int_0^1 dl\int_0^\infty\frac{d\beta}{(1+\beta)^3}\left(\widetilde{\Phi}(\Delta_3)-\widetilde{\Phi}(\Delta_4)\right.\\ &\left.-q_1q_2\,\left(\widetilde{\Phi}'(\Delta_3)-\widetilde{\Phi}'(\Delta_4)\right)\,t^2l\,\left(\frac{t}{1+\beta}-1\right)\right)\\ &+\frac{1}{4q_1^2q_2^2}\int_0^1 dt\int_0^\infty\frac{d\beta}{(1+\beta)^2}\left(\widetilde{\Phi}(-\Delta_5)+\widetilde{\Phi}(-\Delta_6)\right)\\ &+(q_1\leftrightarrow q_2,\;\mu\leftrightarrow\nu)\,,\end{aligned}\tag{95}$$

where

$$\begin{aligned}\Delta_3 &= M_K^2\,\beta+p^2\,\frac{tl}{4}\left(\frac{t}{1+\beta}-1\right)\\ &-q_1^2\,\frac{t^2l(1-l)}{4(1+\beta)}-q_2^2\,\frac{t(1-l)}{4}\left(1-\frac{t}{1+\beta}\right),\\ \Delta_4 &= M_K^2\,\beta+p^2\,\frac{tl}{4}\left(1-\frac{t}{1+\beta}\right)\\ &-q_1^2\,\frac{tl}{4}\left(2-\frac{(1+l)t}{1+\beta}\right)-q_2^2\,\frac{t(1+l)}{4}\left(1-\frac{t}{1+\beta}\right),\\ \Delta_5 &= M_K^2\,\beta+p^2\,\frac{t}{4}\left(\frac{t}{1+\beta}-1\right),\\ \Delta_6 &= M_K^2\,\beta+(2q_1^2+2q_2^2-p^2)\,\frac{t}{4}\left(\frac{t}{1+\beta}-1\right).\end{aligned}\tag{96}$$

For the remainder term we obtain

$$\delta I^{\mu\nu}_{tad}(q_1,q_2)=\int\frac{d^4k}{\pi^2 i}S(k)\,R^{\mu\nu}\,,\tag{97}$$

where

$$\begin{aligned}R^{\mu\nu} =\;& \widetilde{\Phi}\left(-\left(k+\frac{p}{2}\right)^2\right)\left(\frac{q_1^{\mu}(k+q_{12}^{+})^{\nu}}{q_1^2(k+q_{12}^{+})q_2}-\frac{q_1^{\mu}q_2^{\nu}}{2q_1^2q_2^2}\right)\\ &+\widetilde{\Phi}\left(-\left(k+\frac{q}{2}\right)^2\right)\left(-\frac{q_1^{\mu}(k-q_{12}^{-})^{\nu}}{q_1^2(k-q_{12}^{-})q_2}+\frac{q_1^{\mu}q_2^{\nu}}{2q_1^2q_2^2}\right)\\ &+\widetilde{\Phi}\left(-\left(k+\frac{q_1}{2}\right)^2\right)\frac{q_1^{\mu}}{q_1^2}\left(\frac{(k+q_{12}^{-})^{\nu}}{(k+q_{12}^{-})q_2}-\frac{(k+q_{12}^{+})^{\nu}}{(k+q_{12}^{+})q_2}\right)\\ &+(q_1\leftrightarrow q_2,\;\mu\leftrightarrow\nu)\,.\end{aligned}\tag{98}$$

The sum of all remainder terms (84), (89) and (98) vanishes identically, which in turn proofs the manifest gauge invariance of the model.

References

1. W. M. Yao *et al.* [Particle Data Group], J. Phys. G **33**, 1 (2006).
2. A. Palano, Nucl. Phys. Proc. Suppl. **39BC**, 287 (1995).
3. G. V. Efimov and M. A. Ivanov, *The Quark Confinement Model of Hadrons*, (IOP Publishing, Bristol & Philadelphia, 1993).
4. N. A. Tornqvist, Z. Phys. C **68**, 647 (1995) [arXiv:hep-ph/9504372].
5. E. van Beveren and G. Rupp, Eur. Phys. J. C **10**, 469 (1999) [arXiv:hep-ph/9806246].
6. L. S. Celenza, S. F. Gao, B. Huang, H. Wang and C. M. Shakin, Phys. Rev. C **61**, 035201 (2000).
7. M. K. Volkov and V. L. Yudichev, Phys. Atom. Nucl. **64**, 2006 (2001) [Yad. Fiz. **64**, 2091 (2001)] [arXiv:hep-ph/0011326].
8. V. V. Anisovich, V. A. Nikonov and A. V. Sarantsev, Phys. Atom. Nucl. **66**, 741 (2003) [Yad. Fiz. **66**, 772 (2003)] [arXiv:hep-ph/0108188].
9. A. V. Anisovich, V. V. Anisovich, L. G. Dakhno, V. N. Markov, M. A. Matveev, V. A. Nikonov and A. V. Sarantsev, arXiv:hep-ph/0508260.
10. R. L. Jaffe, Phys. Rev. D **15**, 267 (1977).
11. N. N. Achasov, S. A. Devyanin and G. N. Shestakov, Phys. Lett. B **108**, 134 (1982) [Erratum-ibid. B **108**, 435 (1982)]; N. N. Achasov and V. N. Ivanchenko, Nucl. Phys. B **315**, 465 (1989).
12. F. Giacosa, Phys. Rev. D **74**, 014028 (2006) [arXiv:hep-ph/0605191]; F. Giacosa, Phys. Rev. D **75**, 054007 (2007) [arXiv:hep-ph/0611388].
13. D. Black, M. Harada and J. Schechter, Prog. Theor. Phys. Suppl. **168**, 173 (2007) [arXiv:0705.0802 [hep-ph]].
14. A. H. Fariborz, R. Jora and J. Schechter, Phys. Rev. D **76**, 014011 (2007) [arXiv:hep-ph/0612200].
15. J. D. Weinstein and N. Isgur, Phys. Rev. Lett. **48**, 659 (1982); Phys. Rev. D **27**, 588 (1983); Phys. Rev. D **41**, 2236 (1990).
16. T. Barnes, Phys. Lett. B **165**, 434 (1985).
17. G. Janssen, B. C. Pearce, K. Holinde and J. Speth, Phys. Rev. D **52**, 2690 (1995) [arXiv:nucl-th/9411021].
18. O. Krehl, R. Rapp and J. Speth, Phys. Lett. B **390**, 23 (1997) [arXiv:nucl-th/9609013].
19. J. A. Oller and E. Oset, Phys. Rev. D **60**, 074023 (1999) [arXiv:hep-ph/9809337].
20. F. E. Close and A. Kirk, Phys. Lett. B **515**, 13 (2001) [arXiv:hep-ph/0106108].
21. V. Baru, J. Haidenbauer, C. Hanhart, Yu. Kalashnikova and A. E. Kudryavtsev, Phys. Lett. B **586**, 53 (2004) [arXiv:hep-ph/0308129]; Yu. Kalashnikova, A. E. Kudryavtsev, A. V. Nefediev, J. Haidenbauer and C. Hanhart, Phys. Rev. C **73**, 045203 (2006) [arXiv:nucl-th/0512028].
22. C. Hanhart, Yu. S. Kalashnikova, A. E. Kudryavtsev and A. V. Nefediev, Phys. Rev. D **75**, 074015 (2007) [arXiv:hep-ph/0701214].
23. R. H. Lemmer, Phys. Lett. B **650**, 152 (2007) [arXiv:hep-ph/0701027].
24. V. V. Anisovich and A. V. Sarantsev, Eur. Phys. J. A **16**, 229 (2003) [arXiv:hep-ph/0204328].
25. V. V. Anisovich, V. A. Nikonov and A. V. Sarantsev, Phys. Atom. Nucl. **65**, 1545 (2002) [Yad. Fiz. **65**, 1583 (2002)] [arXiv:hep-ph/0102338].
26. D. Morgan and M. R. Pennington, Phys. Rev. D **48**, 1185 (1993).
27. S. Weinberg, Phys. Rev. **130**, 776 (1963); A. Salam, Nuovo Cim. **25**, 224 (1962); K. Hayashi, M. Hirayama, T. Muta, N. Seto and T. Shirafuji, Fortsch. Phys. **15**, 625 (1967).
28. G. V. Efimov, M. A. Ivanov and V. E. Lyubovitskij, Few Body Syst. **6**, 17 (1989) [Acta Phys. Austriaca **6**, 17 (1989)].
29. M. A. Ivanov and V. E. Lyubovitskij, Phys. Lett. B **408**, 435 (1997) [arXiv:hep-ph/9705423].
30. I. V. Anikin, M. A. Ivanov, N. B. Kulimanova and V. E. Lyubovitskij, Z. Phys. C **65**, 681 (1995); M. A. Ivanov, M. P. Locher and V. E. Lyubovitskij, Few Body Syst. **21**, 131 (1996); M. A. Ivanov, V. E. Lyubovitskij, J. G. Körner and P. Kroll, Phys. Rev. D **56**, 348 (1997) [arXiv:hep-ph/9612463]; A. Faessler, T. Gutsche, M. A. Ivanov, J. G. Körner and V. E. Lyubovitskij, Phys. Lett. B **518**, 55 (2001) [arXiv:hep-ph/0107205]; A. Faessler, T. Gutsche, M. A. Ivanov, J. G. Korner, V. E. Lyubovitskij, D. Nicmorus and K. Pumsa-ard, Phys. Rev. D **73**, 094013 (2006) [arXiv:hep-ph/0602193]; A. Faessler, T. Gutsche, B. R. Holstein, V. E. Lyubovitskij, D. Nicmorus and K. Pumsa-ard, Phys. Rev. D **74**, 074010 (2006) [arXiv:hep-ph/0608015].
31. A. Faessler, T. Gutsche, M. A. Ivanov, V. E. Lyubovitskij and P. Wang, Phys. Rev. D **66**, 010001 (2002) [arXiv:hep-ph/0304031].
32. F. Giacosa, T. Gutsche and V. E. Lyubovitskij, Phys. Rev. C **76** (2007) 065204 [arXiv:0710.3403 [hep-ph]].
33. A. Faessler, T. Gutsche, V. E. Lyubovitskij and Y. L. Ma, Phys. Rev. D **76**, 014005 (2007) [arXiv:0705.0254 [hep-ph]]; A. Faessler, T. Gutsche, V. E. Lyubovitskij and Y. L. Ma, arXiv:0709.3946 [hep-ph]; A. Faessler, T. Gutsche, S. Kovalenko and V. E. Lyubovitskij, Phys. Rev. D **76**, 014003 (2007) [arXiv:0705.0892 [hep-ph]].
34. S. Weinberg, Physica A **96**, 327 (1979).
35. J. Gasser and H. Leutwyler, Annals Phys. **158**, 142 (1984).
36. J. Gasser and H. Leutwyler, Nucl. Phys. B **250**, 465 (1985).
37. J. A. Oller, E. Oset and J. R. Pelaez, Phys. Rev. D **59**, 074001 (1999) [Erratum-ibid. D **60**, 099906 (1999), Erratum-ibid. D **75**, 099903 (2007)] [arXiv:hep-ph/9804209]. J. A. Oller, E. Oset, F. Guerrero and J. R. Pelaez, Nucl. Phys. A **663**, 991 (2000) [arXiv:hep-ph/9908494].
38. G. Ecker, J. Gasser, A. Pich and E. de Rafael, Nucl. Phys. B **321**, 311 (1989).
39. G. Ecker, J. Gasser, H. Leutwyler, A. Pich and E. de Rafael, Phys. Lett. B **223**, 425 (1989).
40. K. Kawarabayashi and M. Suzuki, Phys. Rev. Lett. **16**, 255 (1966); Riazuddin and Fayyazuddin, Phys. Rev. **147**, 1071 (1966).
41. S. Mandelstam, Annals Phys. **19**, 1 (1962).
42. J. Terning, Phys. Rev. D **44**, 887 (1991).
43. M. R. Frank, K. L. Mitchell, C. D. Roberts and P. C. Tandy, Phys. Lett. B **359**, 17 (1995) [arXiv:hep-ph/9412219]; R. Jakob, P. Kroll and M. Raulfs, J. Phys. G **22**, 45 (1996) [arXiv:hep-ph/9410304]; A. V. Radyushkin and R. T. Ruskov, Nucl. Phys. B **481**, 625 (1996) [arXiv:hep-ph/9603408]; F. G. Cao, T. Huang and B. Q. Ma, Phys. Rev. D **53**, 6582 (1996) [arXiv:hep-ph/9603330]; I. V. Anikin, A. E. Dorokhov and L. Tomio, Phys. Part. Nucl. **31**, 509 (2000) [Fiz. Elem. Chast. Atom. Yadra **31**, 1023 (2000)]; P. Maris

and P. C. Tandy, Phys. Rev. C **65**, 045211 (2002) [arXiv:nucl-th/0201017]; M. K. Volkov, A. E. Radzhabov and V. L. Yudichev, Phys. Atom. Nucl. **66**, 2143 (2003) [Yad. Fiz. **66**, 2193 (2003)] [arXiv:hep-ph/0210306].
44. T. Mori *et al.* [Belle Collaboration], Phys. Rev. D **75**, 051101 (2007) [arXiv:hep-ex/0610038].
45. H. Marsiske *et al.* [Crystal Ball Collaboration], Phys. Rev. D **41**, 3324 (1990).
46. J. Boyer *et al.*, Phys. Rev. D **42**, 1350 (1990).
47. M. R. Pennington, T. Mori, S. Uehara and Y. Watanabe, arXiv:0803.3389 [hep-ph].
48. M. D. Scadron, G. Rupp, F. Kleefeld and E. van Beveren, Phys. Rev. D **69**, 014010 (2004) [Erratum-ibid. D **69**, 059901 (2004)] [arXiv:hep-ph/0309109].
49. M. Schumacher, Eur. Phys. J. A **30**, 413 (2006) [arXiv:hep-ph/0609040].
50. A. V. Anisovich, V. V. Anisovich and V. A. Nikonov, Eur. Phys. J. A **12**, 103 (2001) [arXiv:hep-ph/0108186].
51. J. A. Oller and E. Oset, Nucl. Phys. A **629**, 739 (1998) [arXiv:hep-ph/9706487].
52. S. J. Brodsky and G. P. Lepage, Phys. Rev. D **24**, 1808 (1981).
53. F. Ambrosino *et al.* [KLOE Collaboration], Phys. Lett. B **634**, 148 (2006) [arXiv:hep-ex/0511031].

Table 1. Electromagnetic decay width $f_0(980) \to \gamma\gamma$: comparison with data and other approaches (quarkonia models ($q\bar{q}$), four-quark models ($q^2\bar{q}^2$) and hadronic approaches).

Approach	Data [44]	Data [1]	Data [45]	Data [46]
$\Gamma(f_0 \to \gamma\gamma)$, keV	$0.205^{+0.095\,+0.147}_{-0.083\,-0.117}$	$0.29^{+0.07}_{-0.09}$	$0.31 \pm 0.14 \pm 0.09$	$0.29 \pm 0.07 \pm 0.12$

Approach	Ref. [51] (hadronic)	Ref. [22] (hadronic)	Ref. [3] ($q\bar{q}$)	Ref. [50] ($q\bar{q}$)	Ref. [48] ($q\bar{q}$)	Ref. [49] ($q\bar{q}$)	Ref. [11] ($q^2\bar{q}^2$)	Our result
$\Gamma(f_0 \to \gamma\gamma)$, keV	0.20	0.22 ± 0.07	0.24	$0.28^{+0.09}_{-0.13}$	0.31	0.33	0.27	0.29 (local) 0.25 (nonlocal)

Table 2. Strong decay width $f_0 \to \pi\pi$: comparison with data and other approaches.

Approach	Data [44] (Belle)	Data [1] (PDG)	Ref. [25] (analysis)	Ref. [37] (hadronic)	Ref. [3] ($q\bar{q}$)
$\Gamma(f_0 \to \pi\pi)$, MeV	$51.3^{+20.8\,+13.2}_{-17.7\,-3.8}$	40 - 100	64 ± 8	18.2	20

Approach	Ref. [7] ($q\bar{q}$)	Ref. [24] ($q\bar{q}$)	Ref. [48] ($q\bar{q}$)	Ref. [6] ($q\bar{q}$)	Our result
$\Gamma(f_0 \to \pi\pi)$, MeV	28	52-58	53	56	69

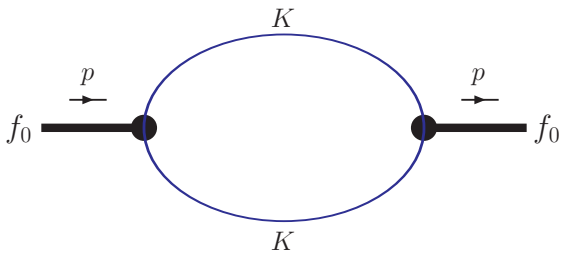

Fig. 1. Mass operator of the f_0 meson.

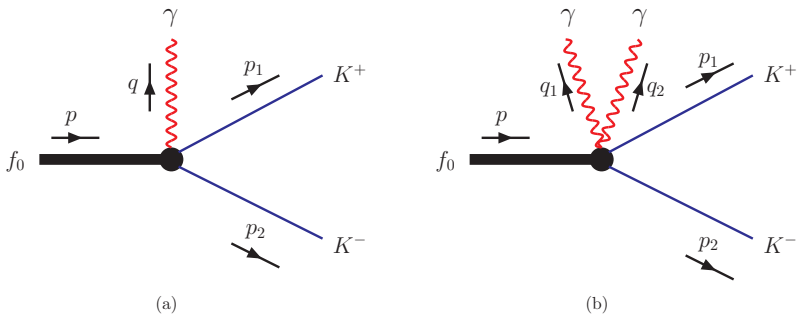

Fig. 2. Electromagnetic vertices generated by the restoration of gauge invariance in the nonlocal case.

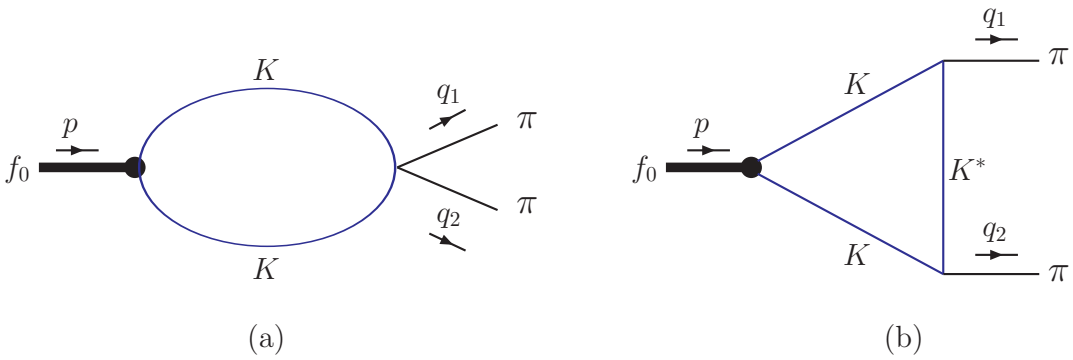

Fig. 3. Diagrams contributing to the strong $f_0 \to \pi\pi$ decay.

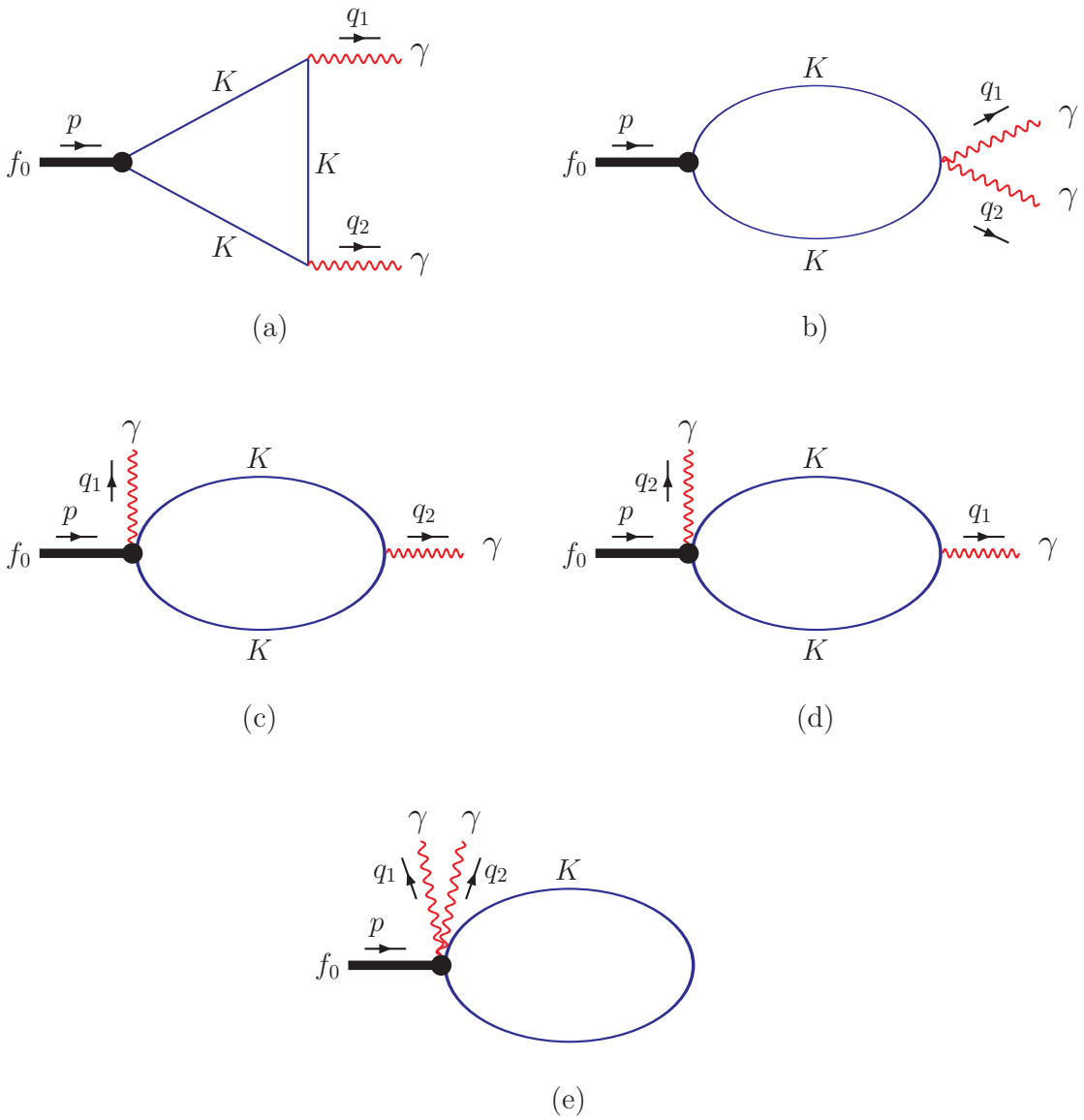

Fig. 4. Diagrams contributing to the electromagnetic $f_0 \to \gamma\gamma$ decay.

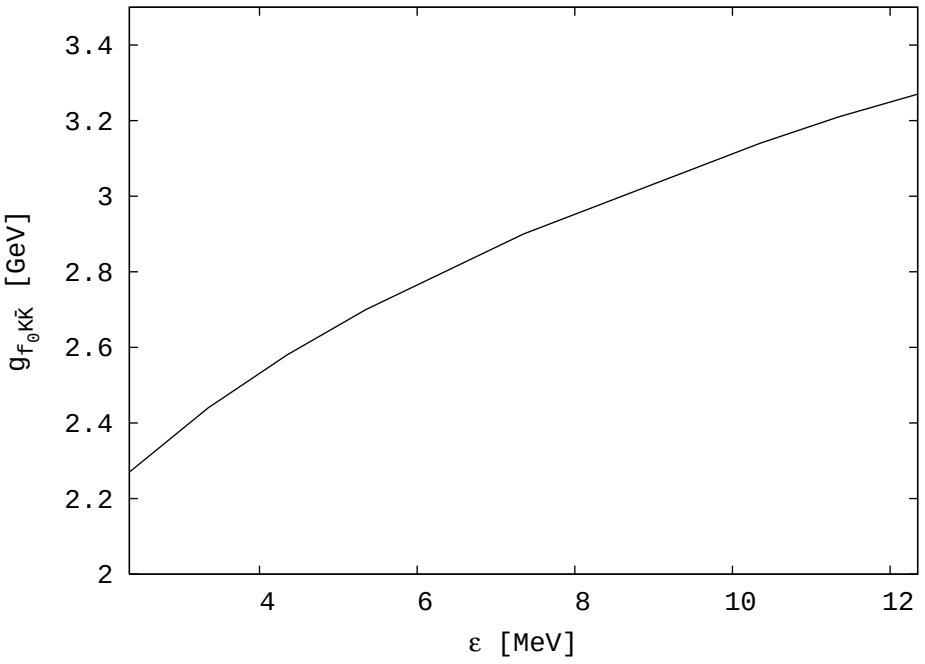

Fig. 5. Coupling constant $g_{f_0K\bar{K}}$ in the local case in dependence on the binding energy ϵ.

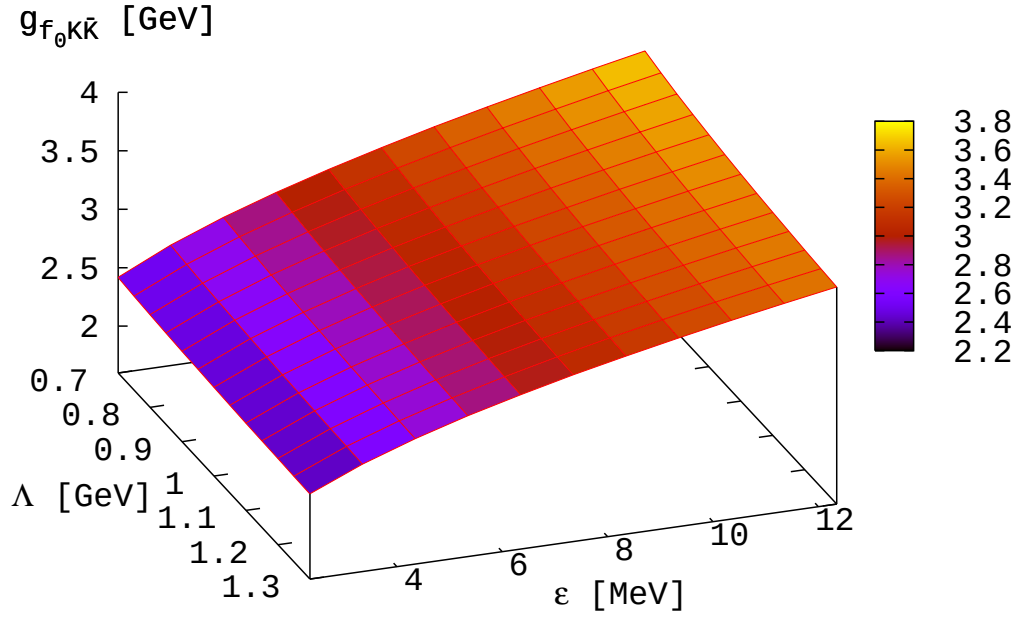

Fig. 6. Coupling constant $g_{f_0K\bar{K}}$ in the nonlocal case in dependence on the binding energy ϵ and the cut-off Λ.

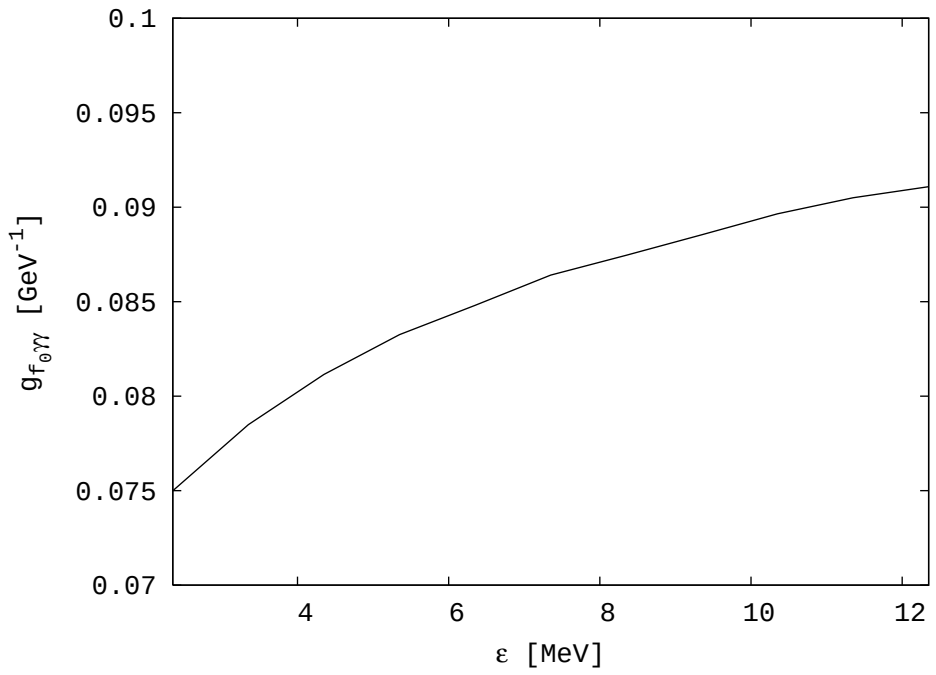

Fig. 7. Coupling constant $g_{f_0\gamma\gamma}$ in the local case in dependence on ϵ.

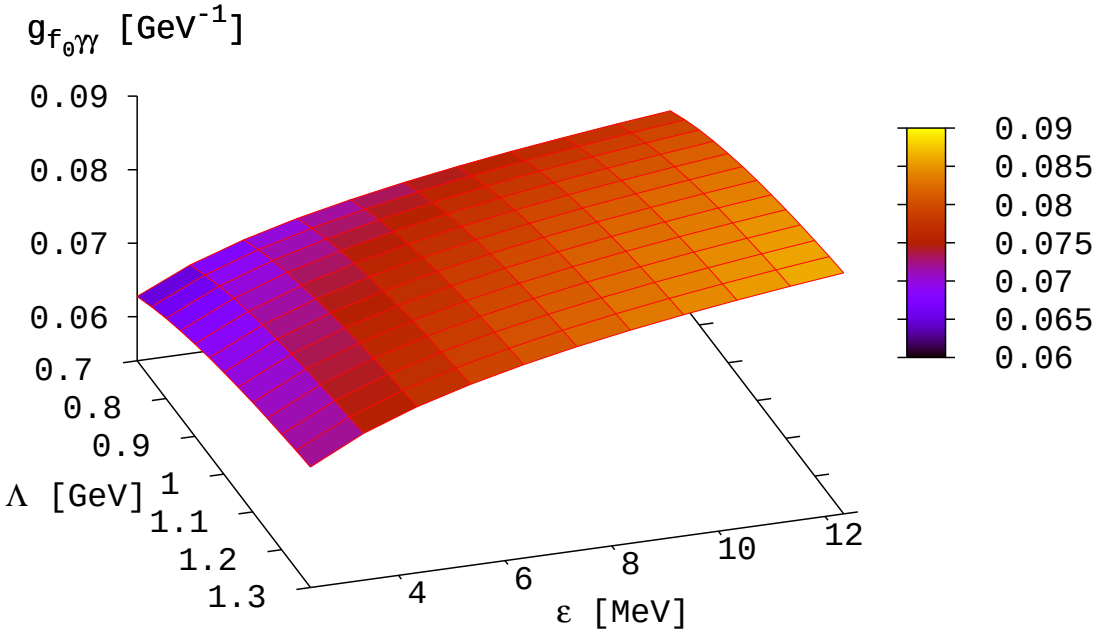

Fig. 8. Coupling constant $g_{f_0\gamma\gamma}$ in the nonlocal case in dependence on ϵ and Λ.

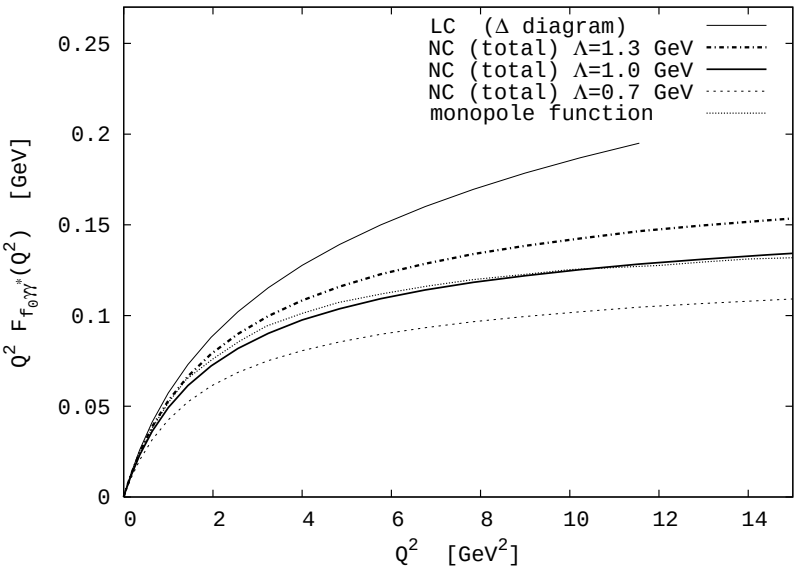

Fig. 9. The form factor $Q^2 F_{f_0\gamma\gamma^*}(Q^2)$ in dependence on Q^2 for the local case (LC). For the nonlocal case (NC) results are given for the triangle (Δ) diagram and for all of Fig. 4 (total). The binding energy is set to ϵ=7.4 MeV for all curves. For the monopole function see the text.

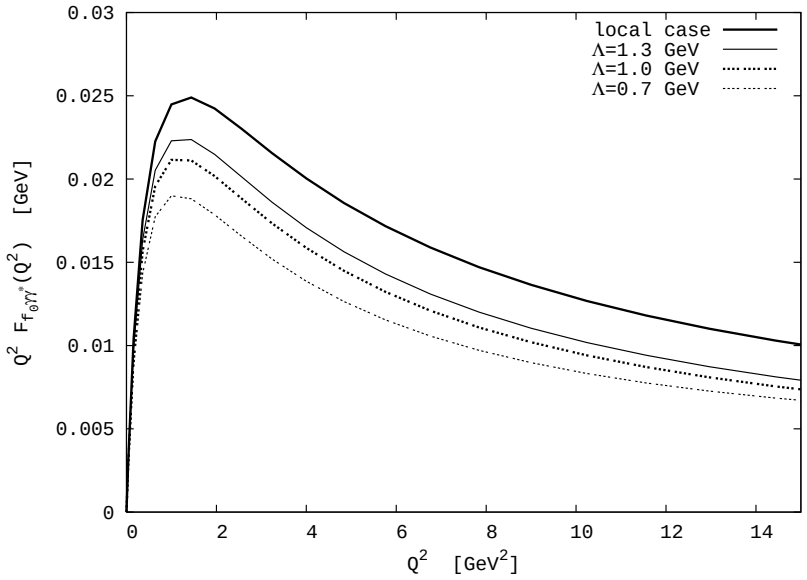

Fig. 10. The form factor $Q^2 F_{f_0\gamma\gamma^*}(Q^2)$ in dependence on Q^2 with the additional monopole form factors $F_{K\bar{K}\gamma}(Q^2)$ at the $K\bar{K}\gamma$ vertices.

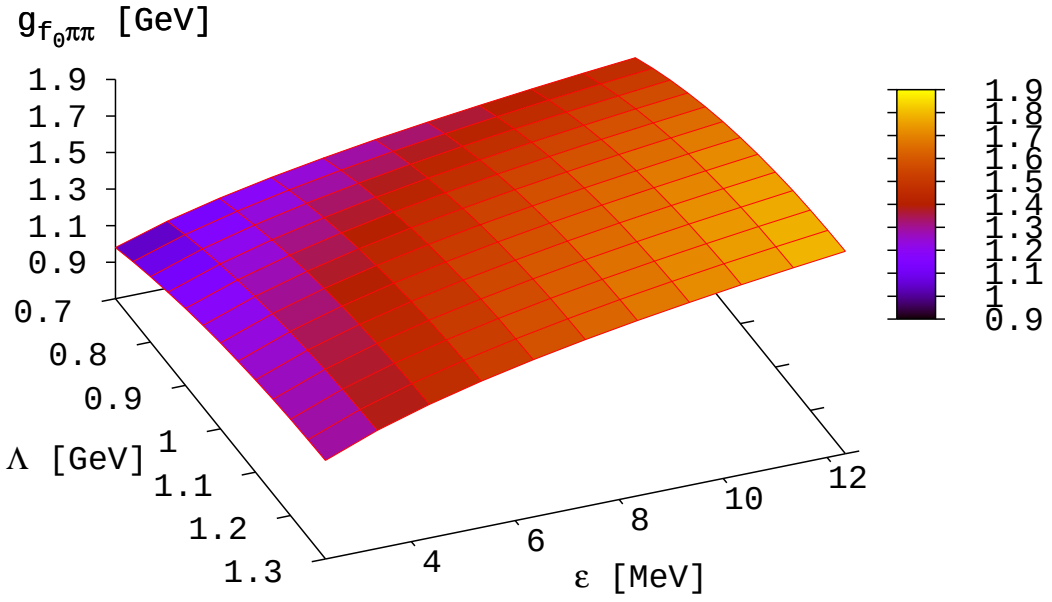

Fig. 11. Coupling constant $g_{f_0\pi\pi}$ in the local case.